Southern Plains Transportation Center
CYCLE 1

FINAL REPORT

2023–2024

USDOT BIL Regional UTC
Region 6

Multifunctional Geosynthetic-Based Stabilization to Increase Coastal Infrastructure Resilience

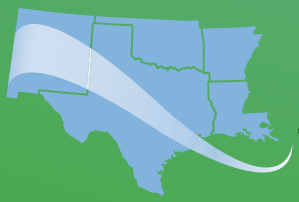

SOUTHERN PLAINS
TRANSPORTATION CENTER

Disclaimer

The contents of this report reflect the views of the authors, who are responsible for the facts and accuracy of the information presented herein. This document is disseminated under the sponsorship of the Department of Transportation University Transportation Centers Program, in the interest of information exchange. The U.S. Government assumes no liability for the contents or use thereof.

Technical Report Documentation Page

1. Report No. CY1-TTI-02	**2. Government Accession No.** [Leave blank]	**3. Recipient's Catalog No.** [Leave blank]
4. Title and Subtitle Multifunctional Geosynthetic-Based Stabilization to Increase Coastal Infrastructure Resilience		**5. Report Date** 01/15/2025 **6. Performing Organization Code**
7. Author(s) Dr. Puneet Bhaskar (PI) – Orcid ID: 0009-0008-0973-9879 Ms. Darlene Goehl (Co-PI) – Orcid ID: 0000-0001-7146-5495 Dr. Anand J. Puppala (Co-PI) – Orcid ID: 0000-0003-0435-6285 Mr. Jaime Suarez (Graduate Student) – Orcid ID: 0009-0003-3019-0415		**8. Performing Organization Report No.**
9. Performing Organization Name and Address Texas A&M Transportation Institute 1111 Rellis Pkwy, Bryan, TX 77807 Zachry Department of Civil and Environmental Engineering, Texas A&M University Engineering Building, 201 Dwight Look, College Station, TX 77840		**10. Work Unit No. (TRAIS)** **11. Contract or Grant No.** 69A3552348306
12. Sponsoring Agency Name and Address Southern Plains Transportation Center 202 West Boyd St., Room 213B The University of Oklahoma Norman, OK 73019		**13. Type of Report and Period Covered** Final Report (09/2023 – 12/2024) **14. Sponsoring Agency Code** [Leave blank]
15. Supplementary Notes Conducted in cooperation with the U.S. Department of Transportation as a part of University Transportation Center (UTC) program.		
16. Abstract Coastal communities of Texas and Louisiana primarily rely on road infrastructure for their transportation and access to goods and services. Due to surge in extreme rainfall and storm events, coastal infrastructure is at pressing risk. The aggressive infiltration of water in highway embankment slopes due to flooding declines its functional and structural performance gradually. Most of the commonly used geosynthetics do not help with drainage under both saturated and unsaturated conditions. A novel geotextile with special hydrophilic and hygroscopic wicking fibers is gaining popularity due to its multiple functions, including separation, reinforcement, gravity drainage, and capillary drainage through wicking action. This research study focuses on understanding the effect of flooding and drainage on interface strength of wicking geotextile, a crucial parameter in the design of reinforced slopes. A large-scale direct shear box was used to conduct interface tests with wicking geotextile. Tests were performed immediately after flooding and after seven days to capture the effects of wicking-induced drainage on interface strength properties. The drainage capability of wicking geotextile was also evaluated at different normal stress levels. Additionally, a finite element model was developed, and numerical analyses were conducted to examine effect of interface strength properties of wicking geotextile on safety factors of slope subjected to flooding. The findings prioritize the use of wicking geotextiles with for better drainage and interface strength to ensure enhanced slope stability under saturated and unsaturated conditions. It also suggests application of wicking geotextiles as part of an integrated flood management strategy for coastal transportation infrastructure to mitigate the effects of storm surges and heavy precipitation.		
17. Key Words Coastal Transportation Infrastructure, Geosynthetics, Interface Testing, Slope Stability	**18. Distribution Statement** No restrictions. This publication is available at www.sptc.org and from the NTIS.	

19. Security Classification (of this report) Unclassified	**20. Security Classification (of this page)** Unclassified	**21. No. of Pages** 63	**22. Price** N/A

Form DOT F 1700.7 (8-72) Reproduction of completed page authorized

MULTIFUNCTIONAL GEOSYNTHETIC-BASED STABILIZATION TO INCREASE COASTAL INFRASTRUCTURE RESILIENCE

FINAL REPORT
SPTC Project Number: CY1-TTI-02

Submitted by
Dr. Puneet Bhaskar (PI)[1]
Ms. Darlene Goehl (Co-PI)[1]
Dr. Anand J. Puppala (Co-PI)[2]
Jaime Suarez (Graduate Student)[2]

Affiliation:
[1]Texas A&M Transportation Institute
[2]Zachry Department of Civil and Environmental Engineering, Texas A&M University

Prepared for
Southern Plains Transportation Center
The University of Oklahoma
Norman, OK

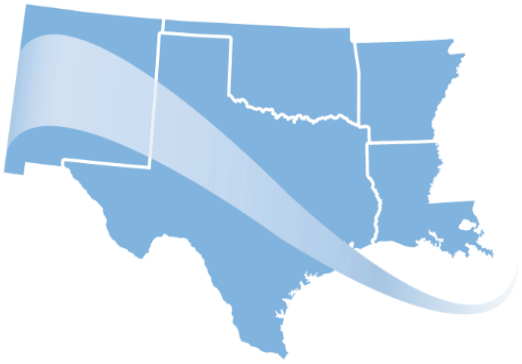

SOUTHERN PLAINS
TRANSPORTATION CENTER

[January 2025]

Acknowledgments

We would like to express our sincere gratitude to the Southern Plains Transportation Center (SPTC) for providing the funding that made this project possible. Their support was instrumental in enabling us to undertake and complete this study successfully. We also extend our heartfelt thanks to the Center for Infrastructure Renewal (CIR) for granting us access to their state-of-the-art laboratory facilities, which were essential for conducting the experiments and achieving the project's objectives. Lastly, we would like to thank all the staff at the Texas A&M Transportation Institute (TTI) for their unwavering support and assistance throughout the project. Their efforts in ensuring the smooth execution and management of the project were invaluable. This report is a result of the collaborative efforts and contributions of everyone involved, and we are deeply appreciative of their dedication and commitment.

Table of Contents

List of Tables

List of Figures

List of Equations

List of Abbreviations and Acronyms

FOS…….. Factor of Safety
GTX…….. Geotextile
GWCC…….. Geotextile Water Characteristic Curve
OMC…… Optimum Moisture Content
SWCC…….. Soil Water Characteristic Curve
UCS…….. Unconfined Compressive Strength
USCS……... Unified Soil Classification System

Executive Summary

Coastal transportation infrastructure plays a pivotal role in the commerce and economic development of a nation. Natural disasters, such as flooding, cause extensive damage to roadways, disrupt transportation systems, and results in substantial economic losses. Currently, approximately 60,000 miles of coastal roadways in the United States are at risk due to storms and flooding. The risk is mainly because of failure of highway embankment slopes due to soil saturation during flooding. Coastal highway slope failures are critical geo-environmental hazard, impacting both the economy and community life. Different types of geosynthetic have been used in slope construction for soil reinforcement. For drainage in slopes, conventional non-woven geotextiles are commonly used however, these geotextiles drain water just through gravity and are effective only in saturated conditions. These limitations necessitate the development of advanced materials with enhanced drainage capabilities. An innovation in this area is the application of wicking geotextiles, which has wicking fibers capable of facilitating lateral drainage in both saturated and unsaturated conditions. Recent research studies have shown their effectiveness in pavement applications, but their performance in embankment slopes, especially under flooding conditions, remains underexplored. Additionally, the interaction between geotextiles and soil, particularly the interface shear strength, plays a critical role in slope stability.

This research study evaluates the performance of wicking geotextiles as drainage and reinforcement elements in highway embankment slopes subjected to extreme flooding events. Through a comprehensive laboratory testing program and numerical analyses, the study assesses the drainage and interface properties of wicking geotextiles and their impact on slope stability. Laboratory interface tests were conducted using a large-scale direct shear apparatus to obtain interface strength properties of wicking geotextiles under varying values of normal stress and degree of saturation. The experimental results were used to develop a 2-D finite element model to perform stability analysis for a slope during and after flooding events. The results highlight the dual benefits of wicking geotextiles in improving both drainage and slope stability in coastal highway embankments subjected to flooding. By providing high interface strength during flooding and enhancing drainage during the drawdown phase, wicking geotextiles can potentially provide an effective solution to address flooding induced embankment slope failures in coastal regions. The findings emphasize the possibility of including wicking geotextiles in infrastructure design to improve its resilience against weather-induced challenges and ensure long-term performance. Furthermore, it provides a foundation for future research and practical applications aimed at optimizing the use of wicking geotextiles in geotechnical engineering, particularly in areas prone to flooding and extreme weather conditions.

Chapter 1. Introduction

General

Coastal regions are vital to the global economy, as almost 50% of the world's major cities are within 50 kilometers of a coastline (Pal et al., 2023). Furthermore, coastal areas tend to have a higher population density compared to regions further inland (Pal et al., 2023). Highways are one of the key drivers of prosperity of urban coastal areas. There are approximately 60,000 miles of coastal highways in the United States (Sharar-Salgado & Brown, 2023).

Coastal areas and their infrastructure are vulnerable to the effects of sea level variability, temperature swings, and precipitation events (Neumann et al., 2015). Intense hurricanes, typhoons and other tropical phenomena are a threat. In recent years, several strong hurricanes have struck the state of Texas, such as Hurricane Harvey in 2017, Hurricane Nicholas in 2021, and more recently Hurricane Beryl in July 2024. Beryl heavily impacted the Houston area with strong winds, over 10 inches of rainfall and significant storm surge, which caused power outages, damage to infrastructure, and travel disruptions. Often, the greatest impact from hurricanes is caused by storm surge, which represents approximately 90 percent of total hurricane-related fatalities (Tate & Frazier, 2013).

One of the dangers to geotechnical structures caused by storm surge and precipitation is soil saturation, which is particularly dangerous to slopes, as it reduces their stability and may cause failure. Jafari and Puppala (2018) noted that one of the factors which influence the probability of slope failure is the intrusion of moisture into the soil. The effects of highway embankment slope failures are severe and far-reaching beyond the immediate human costs, as they can disrupt the flow of commerce, isolate communities, and bring about significant costs for clearance and rebuilding.

Figure 1. Highway embankment slope failure in a coastal area

Wicking geotextile is a recently developed geosynthetic product which combines polypropylene yarns for reinforcement purposes and wicking fibers for drainage. Wicking fabric was first introduced in the 1980's and was originally used for clothing applications. Years later, wicking fibers were incorporated into geotextiles to improve their drainage capabilities. The average diameter of a wicking fiber is between 30 and 50 micrometers, and the spacing between grooves varies between 5 and 12 micrometers (Lin & Zhang, 2018). Wicking fiber is an additive enhanced nylon fiber with a deep grooved cross-section allowing for moisture transport. This fiber has both hydrophilic and hydrophobic elements, which allows it to pull water from the surrounding soil and then transport it along its channels (M. Azevedo & Zornberg, 2013). The large specific surface areas in the wicking fiber allow it to develop suction which absorbs water from the soil into the fiber channels (Guo et al., 2017). While other geotextiles can also drain moisture from soil under certain conditions, such as when the soil is saturated, wicking geotextile can drain moisture both in saturated and unsaturated soil conditions.

Problem Statement

There is currently a pressing need for innovative solutions for application on highway embankment slopes that can rapidly drain water after extreme weather events. Wicking geotextiles are innovative materials that can drain the moisture in embankment soils while providing reinforcement. Most of the current research involving wicking geotextiles focuses on enhancing the performance of pavements and other geotechnical structures. However, there is a lack of studies that focus on studying the effectiveness of wicking geotextile to enhance the performance of embankment slopes. For reinforced earth slopes, one of the main design parameters is interface strength properties of geosynthetic. There is a need for a research study on interface properties of wicking geotextile to understand its efficacy in highway embankments slopes vulnerable to extreme weather events.

Research Hypotheses

To resolve the previously mentioned problem and research gaps, the following hypotheses were formulated:

- The addition of wicking geotextile will improve the interface shear properties of a given soil with geotextile, as measured through large-scale direct shear box testing.
    - Wicking geotextile presence will reduce the water content level in the soil over a given time when compared to soil specimens without wicking geotextile reinforcement. This improvement will lead to a higher factor of safety for a highway embankment slope.

Research Objectives

To prove the previously mentioned hypotheses, a detailed evaluation of the performance of wicking geotextile is required using a combination of testing methods. For this reason, the following thesis research tasks were formulated with three main objectives:

- To experimentally determine interface strength properties of wicking geotextile under different saturation and normal stress levels.
- To study the effect of wicking induced drainage on interface strength properties of geotextile.
- To evaluate effect of wicking geotextile reinforcement on the overall stability of a highway embankment slope through numerical modeling.

Chapter 2. Literature Review

Coastal Flooding

Flooding caused by storm surges significantly increases the vulnerability and reduces the functionality of coastal transportation infrastructure. Several studies have analyzed the effects of flooding on coastal road infrastructure. A study by Azevedo de Almeida & Mostafavi, (2016) noted that the total amount of precipitation in coastal areas was expected to rise by 10 to 20% in the following decades, which would lead to higher water tables and reduced soil storage capacity. The study specifies that increased flooding will damage roads due to soaked bases and subgrade conditions, causing excessive deformation and soil failure, ultimately leading to road closure. A research study by Johnston et al. (2021) identified five mechanisms that can drive the collapse of highway embankment slopes during flooding: Internal erosion, live loading, scour, sliding, and wetting front development. Additionally, it identified rapid drawdown as one of the most common causes of slope failure, as the floodwaters which had a stabilizing effect on the slope are suddenly withdrawn. Soils with high permeability are less vulnerable to the effects of rapid drawdown.

Another study analyzed the possible causes behind an embankment failure, finding that the untreated soil in the slope lost strength due to a combination of wetting-drying cycles and precipitation (Boluk et al., 2021). Briggs et al., (2017) pointed out that the main cause of highway embankment failures is increase in pore water pressure, caused by loss of soil suction or by water infiltration, that results in a reduction in effective stress. According to the study, a precipitation-induced rise in pore pressure is likely to cause a shallow slope failure, and it can be mitigated through the usage of drainage measures or the application of low permeability fill.

Applications of Wicking Geotextile

One of the primary roles of wicking geotextiles is to minimize capillary water buildup by limiting the rise of capillary water and draining it from the soil through suction, also known as capillary pressure (Bai et al., 2021). In pavements, wicking geotextiles draw water from the soil and transport it along the material through capillary suction (Zaman et al., 2024). This capillary pressure, generated by the wicking geotextile, leads to a gradual reduction in the saturation level of both the geotextile and the surrounding soil (Lin & Zhang, 2015). Small soil column infiltration tests (M. M. de Azevedo, 2012) demonstrate that wicking geotextiles offer superior lateral drainage compared to conventional geotextiles, thanks to their ability to dissipate capillary barriers. This was confirmed through microscopy, which observed moisture within the channels of the wicking fibers.

There has been plenty of research surrounding the use of wicking geotextile in improving pavement subgrade strength. For example, a study by Biswas et al. (2021) tested the effectiveness of wicking geotextile in an expansive soil. As part of laboratory tests, two boxes were filled with soil and a wicking geotextile was placed in one of the boxes with the end of the geotextile exposed to the atmosphere, so it could remove the humidity from the soil. Both boxes were then filled with water and left for 7 days with similar initial conditions. These laboratory tests were combined with field tests where pavement sections were made with sensors placed within them to monitor moisture content for one month. The study discovered that moisture content values of soil were lower in both laboratory and field tests if the soil was reinforced with wicking geotextile, which was responsible for the moisture reductions which in turn caused stiffness improvements.

Galinmoghadam et al., (2022) analyzed the usefulness of wicking geotextile in pumping reduction for pavements. Four drainage tests were conducted for different scenarios with saturated compacted soil in boxes. Additionally, three sections in a stretch of road were instrumented, and wicking geotextile was placed in two of the sections. The resulting drainage was then evaluated in all test sections for 3 years. Test results indicated that the wicking geotextile drained capillary water under unsaturated conditions, preventing the development of positive pore pressure in soils caused by traffic loads, which would have produced pumping damage. Additionally, exposing the end of the wicking geotextile to the atmosphere drastically improved its performance. In addition to pumping mitigation, wicking geotextile has also been used to prevent frost boils in a road in Alaska (Lin et al., (2017). The pavement section was instrumented and monitored for 5 years. The researchers found that the wicking geotextile remained effective in removing the water from the road, solving the frost boil problem.

Several studies have also considered the applications of wicking geotextile on pedestrian corridors. A recent study by Luo et al. (2024) compared the effects of one-directional and two-directional wicking geotextile with an experiment on a pedestrian corridor. Both types of geotextiles were placed over the subgrade, and moisture readings were collected on a weekly basis for the two sections, as well as a control section. The test results compiled over the span of a year showed that the two-dimensional wicking geotextile caused the highest moisture dissipation. The section with the one-dimensional wicking geotextile presented slightly higher moisture values, while the control section showed very high moisture values and strong variations during times of presumed rainfall. Lower moisture content values corresponded with increases in the resilient modulus for the sections with geotextile.

Geotextile has also been used for railway applications. As an example, a railway section was constructed over an embankment reinforced with both non-wicking and wicking geotextile. Moisture sensors were installed in both reinforced section and control section and were used to collect water content data for 15 months. The moisture sensor data indicated that the reinforced section had little change in moisture content in the specified timeframe, while the control section had significant seasonal variations in moisture content. This indicated that the wicking geotextile had shown improved drainage in the embankment. This would in turn increase soil suction which suggests higher soil shear strength (Alvarenga et al., 2021).

Interface Properties of Geotextiles

The interface properties of geotextiles have been widely studied by researchers in the past. The interface behavior of a soil-geotextile interface can be measured through direct shear tests and pullout tests. For example, a study by Anubhav & Basudhar (2010) focused on the shear-displacement behavior of the soil-geotextile interface using two different geotextiles that reinforced a poorly graded (SP) sandy soil. Results from the direct shear showed that shear strength was higher in the test with coarse textured geotextile compared to the test with a fine textured geotextile. Test results were used to back-calculate model parameters that would predict soil-geotextile behavior.

Lopes & Silvano (2010) carried out four direct shear tests at the same stress level, calculating the interface coefficient, which is determined by the ratio between the maximum soil/geotextile shear stress and the maximum soil/soil shear stress. This was combined with three pullout tests which also determined the interface coefficient. Comparing the resulting values, the interface coefficient obtained through pullout tests was 55% of the coefficient obtained through direct shear tests. As a result, the authors conclude that direct shear tests may not accurately predict

pullout behavior due to the influence of geotextile deformation on the interface behavior, which is not considered in direct shear tests. Khoury et al. (2011) used a modified shear testing device to determine the effect of suction on the soil-geotextile interface. The study found that the soil-geotextile interface featured slightly higher strain softening and dilation compared to soil specimens. Furthermore, the increased normal stress was correlated with a non-linear increase in the interface shear strength in the soil-geotextile tests, while higher suction was correlated with increases in interface shear strength and interface adhesion, as well as reductions in horizontal displacement.

The determination of accurate peak interface strength properties can be difficult, as there are a multitude of factors which may affect the test results (Lee & Manjunath, 2000). Large scale direct-shear tests with three different geotextiles indicate boundary and testing conditions can influence the obtained result, while lateral distortion and sagging may affect the results from a standard direct shear box. For this reason, measures should be taken to maintain the in-plane state of the geotextile. Furthermore, the results from reverse direct shear tests in this study show that the residual interface shear strength seems to approach a constant value as the geotextile openings become clogged with soil particles.

While the interface strength properties of various geotextiles have been extensively studied, limited research has focused on the effects of drainage on this interface strength. Most investigations into wicking geotextiles emphasize their drainage properties, leaving the combined effects of drainage and interface strength largely unexplored. Understanding the interaction between these factors is essential for enhancing the performance of geotextiles in geotechnical applications, particularly for embankment slopes where both drainage and interface strength are critical to ensuring stability and long-term durability.

Numerical Modeling of Wicking Geotextile

Numerical modeling is frequently used to predict the behavior of pavement sections with and without wicking geotextiles. Commercial finite element software is commonly employed to model the effects of wicking geotextiles. Lin et al. (2021) developed a numerical model using ABAQUS finite element software. They applied a coupled hydro-mechanical model to simulate seasonal variations in the resilient behavior of the base layer aggregate. The model represented a 5.5 m wide road with a 1:3 slope and three pavement layers: asphalt concrete, base course, and subgrade. Precipitation data were used to determine the infiltration rate, while the Penman-Monteith method was applied to calculate evaporation values, integrating all climate factors into a single equation. The simulation analyzed three scenarios: no geotextile in case 1, a non-wicking geotextile in case 2, and a wicking geotextile in case 3. The results showed that non-wicking geotextiles failed to drain sufficient water from the pavement, leading to excess water accumulation and negatively affecting the resilient modulus of the soils. In contrast, the drainage properties of wicking geotextiles facilitated proper moisture drainage, resulting in a higher resilient modulus compared to both the control and non-wicking geotextile cases.

The hydraulic properties of wicking geotextiles were investigated in a study by Lin et al. (2019), which involved a series of tests on the material. To determine the Geotextile Water Characteristic Curve (GWCC) in the in-plane direction, a capillary rise test was conducted for suction values below 10 kPa, a pressure plate test was used for suction values between 10 and 1500 kPa, and a salt concentration test was performed for suction values above 1500 kPa. The in-plane GWCC was modeled as a segmented function, requiring two sets of parameters. The GWCC of a non-wicking geotextile was adopted as the cross-plane curve for the wicking geotextile, as both materials share the same Apparent Opening Size. Additionally, the

geotextile's permeability function was determined by using the saturated permeability value from a constant head test for the in-plane direction and manufacturer specifications for the cross-plane direction, along with the previously obtained GWCC. These hydraulic properties were then incorporated into an ABAQUS model for a pavement section. The simulation results showed that the wicking geotextile reduced the water content in the soil by 2%, leading to a threefold increase in the resilient modulus of the geomaterial.

Jiang et al. (2024) used COMSOL to model the role of wicking geotextile in preventing frost heave in pavements. The model, based on a real pavement section, was validated by installing sensors in the pavement and running simulations for a scenario without wicking geotextile. When wicking geotextile was added to the model, it was represented as a material, with its wicking action modeled as a 200 kPa pressure head applied as a boundary condition at the contact point between the geotextile and the slope surface. After 200 simulated days, the results showed approximately 30 mm of frost heave in the model without geotextile, compared to 10 mm in the model with the reinforced geotextile. The frost depth remained the same in both models. These results suggest that the addition of wicking geotextile delayed the onset of frost heave and reduced the total amount of frost heave in the pavement.

Chapter 3. Materials and Methodologies

Soil Characterization Tests

General

The primary objective of this research study is to evaluate the interface strength and drainage characteristics of wicking geotextile-reinforced soils. For this project, locally sourced soil, procured from a vendor, was used for laboratory testing. This chapter outlines the laboratory characterization tests conducted to classify the soil and determine its fundamental and engineering properties. Tests such as Atterberg limits, Standard Proctor, and sieve analysis were performed following ASTM standards. Additionally, a soil water characteristic test was conducted on soil using a Tempe pressure cell and a dew point potentiometer. The mechanical and hydraulic properties of the wicking geotextile, provided by the vendor, are also detailed. Furthermore, this chapter describes the large-scale direct shear apparatus employed for interface shear strength testing, along with the experimental program, testing methodology, and details of numerical studies conducted in this research study.

Atterberg's Limits

The Atterberg limits of soil are fundamental indicators of a soil's consistency and its behavior under varying moisture conditions. Two types of tests were performed with the objective of determining the liquid and plastic limits of the soil, as well as the plasticity index. The liquid limit and plastic limit values were determined using ASTM 4318 method. The plasticity index value was determined by deducting the plastic limit from the liquid limit. These test results are summarized in the Table 1.

Figure 2. Casagrande device used for the liquid limit test

Table 1. Atterberg's Limits of Soil

Parameter	Value
Liquid Limit (%)	25
Plastic Limit (%)	15
Plasticity Index (%)	10

Grain Size Distribution

The wet sieve and hydrometer tests were conducted on the soil specimens according to the ASTM D422 method. In the wet sieve test, the soil was passed through a series of standard sieves with varying aperture sizes, using water to help finer soil particles pass through the sieves. This method provides a more accurate determination of the material's grain size distribution. The objective of this test is to classify the soil based on the predominant types of soil particles. Based on the results from Atterberg's limit tests and the grain size distribution curve, the soil was classified as silty clayey sand (SM-SC) according to the Unified Soil Classification System.

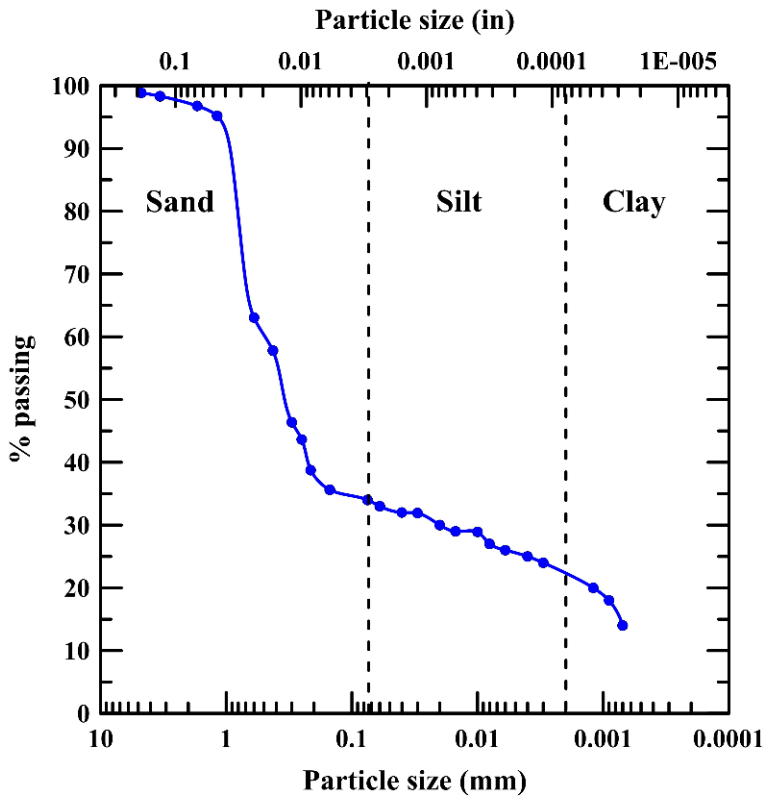

Figure 3. Grain size distribution curve of soil

Standard Proctor Compaction Test

The goal of the standard Proctor test is to determine the maximum dry unit weight (MDUW) and optimum moisture content (OMC) of the soil. To obtain the compaction parameters of test soil, Standard Proctor test was conducted as per ASTM 698 standard test. As shown in Figure 4, the test yielded OMC and MDUW values of 13.4% and 20.2 kN/m^3, respectively.

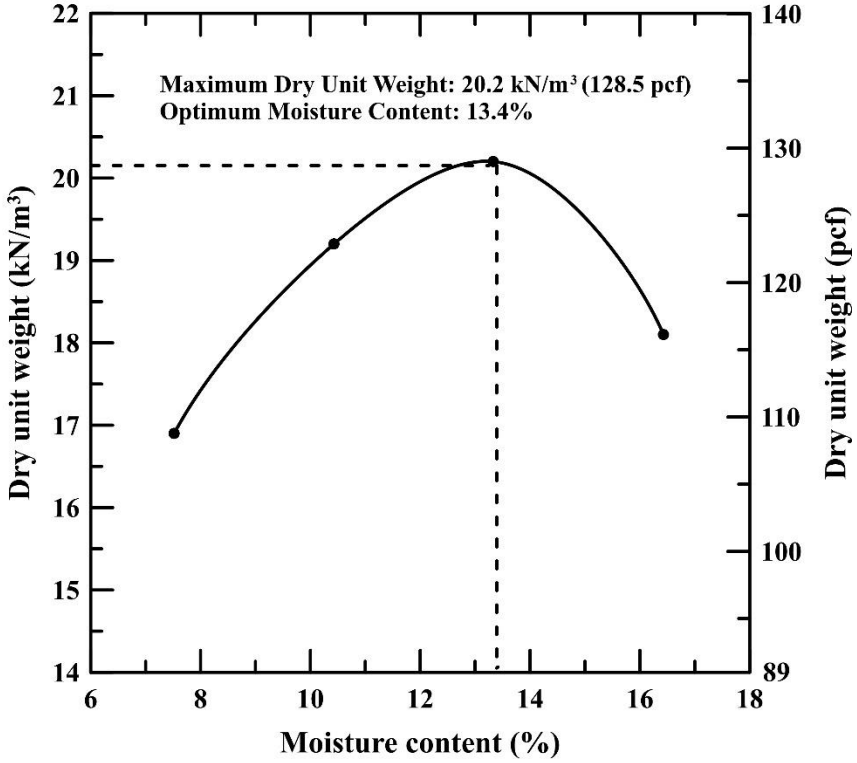

Figure 4. Dry density-moisture content relationship of soil from Standard Proctor test

Unconfined Compressive Strength

A unconfined compressive strength (UCS) test was conducted on the device shown on Figure 5 to determine the unconfined compressive strength of the soil. The test was done according to ASTM 2166 method. Soil specimens were compacted at 90% of maximum dry density and corresponding moisture content on wet side of the Proctor compaction curve. The test yielded a UCS value of 93 kPa.

Figure 5. UCS Sample before test

Table 2. Unconfined Compressive Strength test results

Test	UCS (kPa)
1	92.9

Soil Water Characteristic Curve Test

The Soil Water Characteristic Curve (SWCC) describes the relationship between the amount of water in a soil and matric suction. This curve is required to simulate water distribution and flow in partially saturated soils (Tuller et al, 2004). The SWCC was obtained through the combination of data from two different test methods. Suction values between 0 and 450 kPa were obtained through a Fredlund SWCC device (Figure 6) whereas, SWCC data for suction values over 450 kPa were obtained using a WP4C Dewpoint Potentiometer (Figure 7).

Figure 6. Fredlund device used in SWCC test

Figure 7. Potentiometer used in SWCC test

The values obtained from tests were best fitted using Fredlund and Xing (1994) model parameters and is shown in Figure 8. The parameters that provided the best fit to experimental values can be found in Table 3. The Fredlund-Xing equation for a SWCC is defined in Equation 1, as expressed by Qian & Rahardjo, (2016).

$$\theta(\Psi) = \left[1 - \frac{\ln\left(1 + \frac{\Psi}{C_r}\right)}{\ln\left(1 + \frac{10^6}{C_r}\right)}\right] \frac{\theta_s}{\left[\ln\left(1 + \left(\frac{\Psi}{a}\right)^n\right)\right]^m}$$

where,

Ψ represents matric suction,
C_r represents a suction-related parameter that is usually kept as 1500 kPa,
θ represents water content,
θ_s represents saturated water content, and
a, n and m represent fitting parameters.

Equation 1. SWCC Curve equation

Table 3. Soil Water Characteristic Curve fitting parameters

Fitting parameter	Value
a	14
n	0.6
m	1.2
θ_s (%)	23

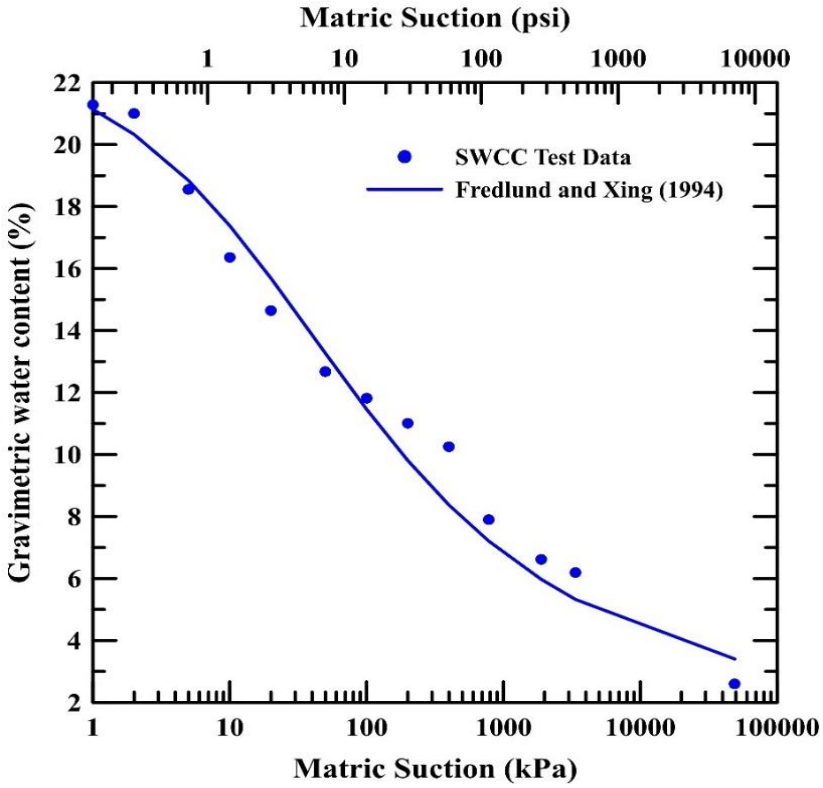

Figure 8. Soil Water Characteristic Curve of the tested soil

Geotextile Properties

The wicking geotextile, as shown in Figure 9, used for the tests was a Mirafi® H2Ri geotextile manufactured by SolMax. Table 4 contains the technical data sheet including key mechanical and physical properties of wicking geotextile used in this study.

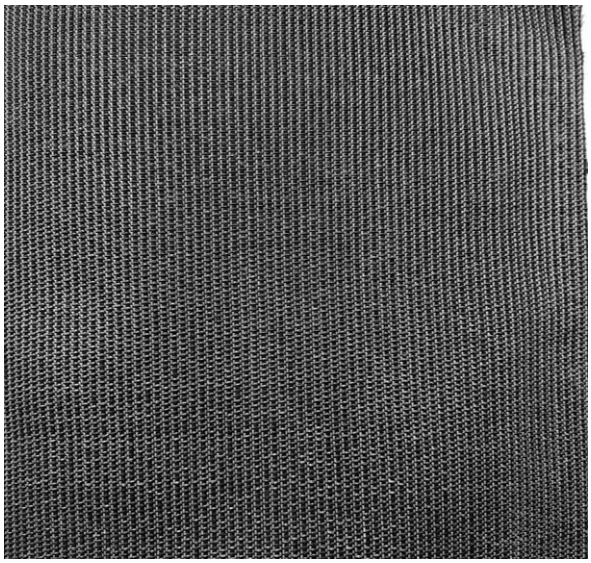

Figure 9. Mirafi H2Ri Wicking Geotextile

Table 4. Wicking geotextile properties (From Solmax)

Geotextile Property	Minimum average roll value
Initial Wide Width Tensile Strength (kN/m)	77
Wide Width Machine Direction Tensile Strength @2% strain (kN/m)	7
Wide Width Cross-Machine Direction Tensile Strength @2% strain (kN/m)	15.8
	Maximum opening size
Apparent opening size (mm)	0.425
	Minimum Roll Value
Permittivity (1/s)	0.4
Flow Rate (l/min/m^2)	1222
	Typical Value
Pore size (050) (microns)	180
Pore size (060) (microns)	234
Pore size (095) (microns)	391
	Minimum Test Value
Wet Front Vertical Movement (24 minutes) (in)	6
Wet Front Horizontal Movement at zero gradient (983 minutes) (in)	73.3
	Typical Roll Value
Roll Dimensions (width x length) (m)	4.59 x 91.44
Roll Area (m^2)	418

Interface Shear Strength Tests

Large Scale Direct Shear Apparatus

The equipment used for the large-scale interface tests includes a top and bottom shear box, horizontal and vertical load cells, an electrical cabinet, Linear Variable Differential Transformer (LVDT), and a control panel (Figure 10). The system is connected to a computer that is used to manage its operations. Both load cells are equipped with LVDT transducers, which measure linear displacements in the direction in which they are placed. The shear box, consisting of an upper and lower section, measures 305 mm (12 in) square with a total height of 203 mm (8 in). During the shearing phase, the lower section is moved horizontally while the upper section is restrained from vertical and horizontal movement. The soil sample in the lower box can be inundated by enclosing it within a sealed chamber. Additionally, the equipment's design accommodates the installation of moisture and suction sensors within the soil sample during testing.

Figure 10. Large Scale Direct Shear Test Setup

Testing Program and Methodology

A total of 18 large-scale interface shear tests were performed in this research study, and all these tests were performed in full compliance with ASTM D5321 standards. Tests were conducted at different moisture levels with and without wicking geotextile interface layer. Following are the six test scenarios that were used for the experimental program.

I. Optimum moisture content, without geotextile.
II. Optimum moisture content, with geotextile.
III. Flooding conditions, without geotextile.
IV. Flooding conditions, with geotextile.
V. 7 Days after flooding, without geotextile.
VI. 7 Days after flooding, with geotextile.

Three tests with normal stress levels of 50, 100, and 200 kPa were conducted for each test combination for unreinforced or control and reinforced soil specimen. The process of testing a typical soil specimen in the present experimental program can be split into the following five steps:

Step 1: Specimen Preparation

The geomaterial, which was dried in an oven for at least 24 hours, was mixed with the required amount of water based on the specified density and moisture content values. Considering a relative compaction of 90% for the soil samples and using the wet side of the proctor curve for soil specimen preparation to account for drying during the compaction process, the target dry density of the soil was determined to be 19 kN/m³ (1.9 gm/cc), with a corresponding gravimetric moisture content of 15.5%. After the soil was evenly mixed, any larger clumps were broken down. To ensure the soil was uniformly mixed at the correct moisture content, water content measurements were taken from different locations within the mixture. The soil mixture was then

compacted in two layers in the lower box of the large direct shear setup using a Proctor hammer.

During the compaction of the second layer, three moisture sensors were placed in the bottom box approximately 2.5 cm below the interface, as shown in Figure 11. Once the sensors were positioned, compaction of the second layer was completed. Holes were punctured in the wicking geotextile so it could be fastened to the top box with screws, as depicted in Figure 12. The top box was then placed on top of the bottom box, with the geotextile tightly positioned at the interface (Figure 13). About 15 centimeters of the geotextile was left outside the box and exposed to the external environment to facilitate capillarity drainage. The soil in the top box was then compacted in two layers (Figure 14), and the top cap was placed above it.

Figure 11. Moisture sensors placed in the bottom box

Step 2: Soil Inundation with Water

For tests where flooding conditions were simulated, the shear box was completely sealed to avoid leaks. Afterward, the material in the lower shear box and a part of the upper box was inundated by filling the water tub located in the apparatus. The water was then kept for 24 hours until it was drained through a valve at the bottom of the apparatus.

Figure 12. Geotextile fastened to top shear box

Figure 13. Wicking geotextile clamped to the shear box

Step 3: Consolidation

After compaction of soil in the shear box, the soil specimen was subjected to consolidation under different normal stresses for 24 hours. The stresses applied on the soil specimens were 50 kPa, 100 kPa and 200 kPa. For tests with flooding conditions, the consolidation process was started and completed before the sample was inundated.

Step 4: Drainage using Wicking Geotextile

For tests with wicking geotextile, specimens were allowed to drain by wicking action for 7 days. Moisture data was continuously recorded by the sensors during drainage. Any exposed area of soil was covered up to avoid losses of moisture to the surroundings.

Step 5: Shearing

The soil sample was then subjected to shearing for 24 hours at a rate of approximately 0.03 mm/min until the shear displacement reaches 46 mm, which represents 15% shear strain. After

this level was reached, the test stops automatically, and the soil specimen was removed. The geotextile was not reused for future tests.

Figure 14. Soil following compaction

Numerical Seepage and Slope Stability Analysis

General

One potential cause of slope failure in coastal regions is the drawdown that occurs following a flooding event. The effectiveness of wicking geotextile in stabilizing a highway embankment slope post-flooding was evaluated through seepage and slope stability analyses. The performance of the geotextile was assessed based on its ability to reduce pore water pressure and enhance the slope's factor of safety through reinforcement. A two-dimensional plane strain model of the embankment slope with different slope angles was developed using a commercially available finite element software.

Slope Geometry and Boundary Conditions

A total of 12 embankment slope models were created which incorporated three different slope angles and four distinct reinforcement configurations. In all models, the total slope height was kept as 4 m, while the length of the slope varied depending on the slope angle. The number of layers and their spacing were determined by the slope configuration and soil type. It is important to note that no separate reinforcement design was carried out for the slopes. The spacing and length of the geotextile were chosen based on design studies with similar slope geometries and soil properties. Each layer of wicking geotextile in all models had a length of 9 meters. The first configuration included two reinforcement layers spaced 2 meters apart, the second configuration had four layers spaced 1 meter apart, and the third configuration consisted of 8 geotextile layers spaced 0.5 meters apart. The fourth configuration served as the control, with no wicking geotextile reinforcement.

The initial water table was positioned at the bottom of the embankment slope. The model was meshed using unstructured quadrilateral and triangular elements. Figure 15 shows the model with a 2:1 slope, referred to as Slope 1. Models with 1.5:1 slope (Slope 2) and 1:1 slope (Slope

3) are shown in Figures 16 and 17, respectively. The lower section of the slope model was restrained in both horizontal and vertical directions, while the lateral boundaries were constrained only horizontally. For seepage analysis, a no-flow hydraulic boundary condition was applied to the base of the model.

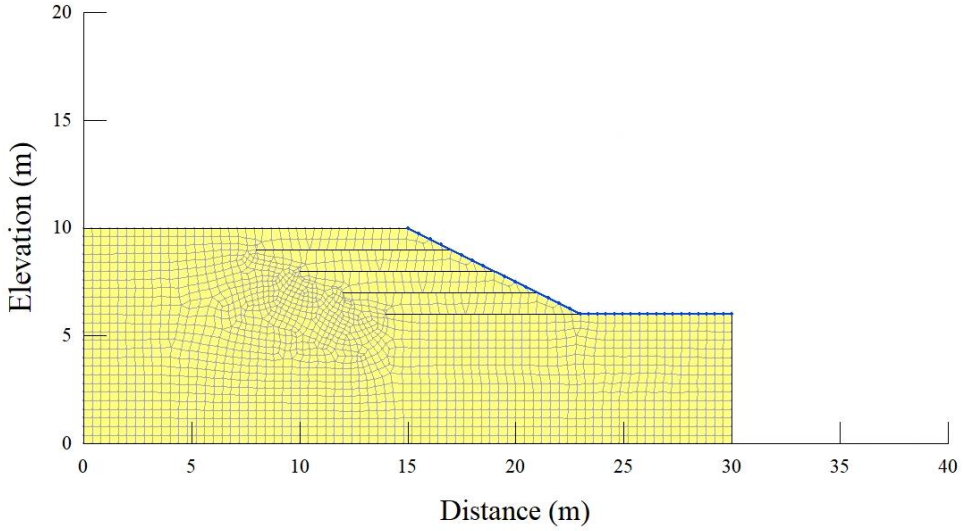

Figure 15. Slope 1 with mesh elements

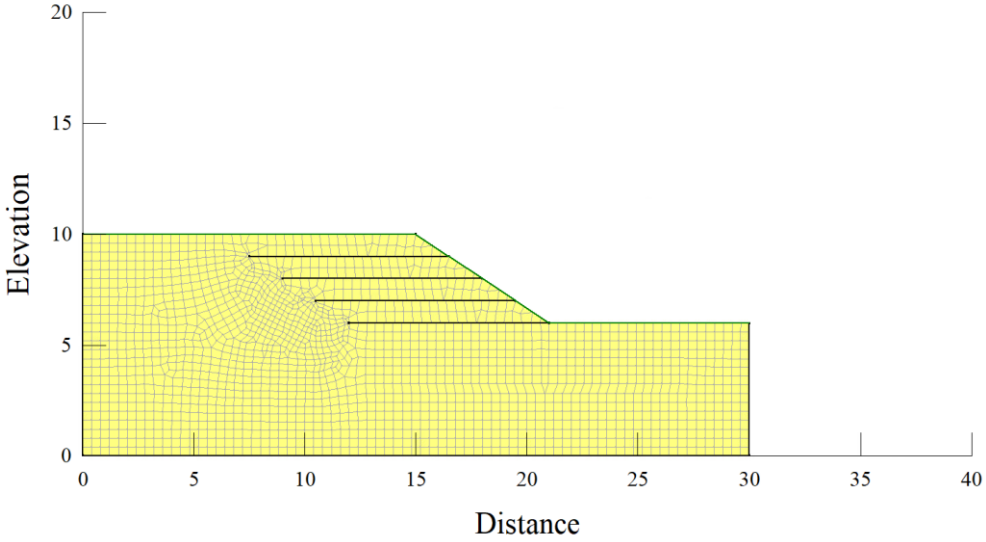

Figure 16. Slope 2 with mesh elements

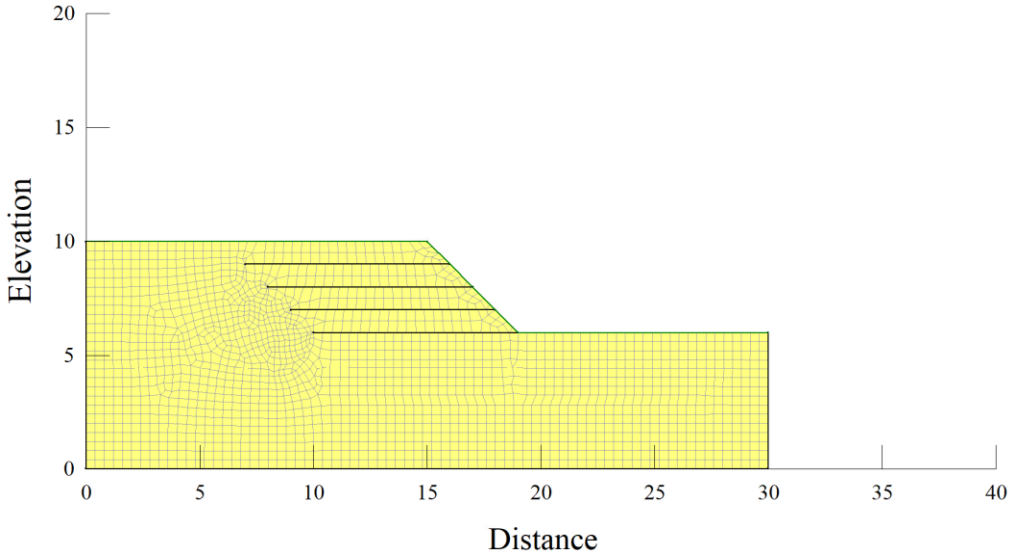

Figure 17. Slope 3 with mesh elements

Material Model

Soil was modeled using Mohr-Coulomb constitutive model and strength parameters were obtained from interface shear tests carried out as part of this research. The properties of the reinforcement layers were estimated from the interface properties of the geotextile obtained in the direct shear tests, and from manufacturer data. The interface properties are used to calculate pullout resistance in the modeling software through the following equation:

$$PR = (SIA + \sigma_v' tan\delta)SAF$$

Where PR corresponds to pullout resistance, SIA is interface adhesion, σ'v represents effective overburden stress, δ is interface friction angle and SAF is surface area factor. The surface area factor is kept at the default value of 2.

Equation 2. Pullout resistance as calculated in GeoStudio

For the soil layers, the SWCC was obtained from laboratory SWCC test, and the hydraulic conductivity curve was determined from the SWCC and the grain size distribution. For the case of the geotextile, the hydraulic curves were taken from Lin et al., (2019) The thickness of the geotextile layers present in the model is 1.6 millimeters. A close-up of the model geometry (Figure 18) displays a geotextile layer.

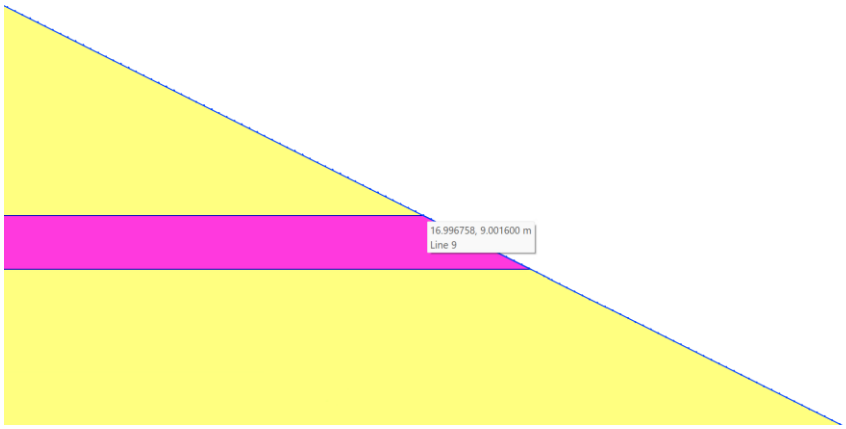

Figure 18. Close-up of wicking geotextile layer

Incorporating the geotextile as a material is expected to provide a more accurate representation of the wicking action, compared to modeling it as a constant pressure head or water flux boundary condition. Although this approach was previously not considered due to the challenges in obtaining the geotextile's hydraulic parameters, the determination of these parameters has now made it feasible. Figure 19 presents a comparison of the in-plane hydraulic conductivity of the geotextile with the hydraulic conductivity of the soil.

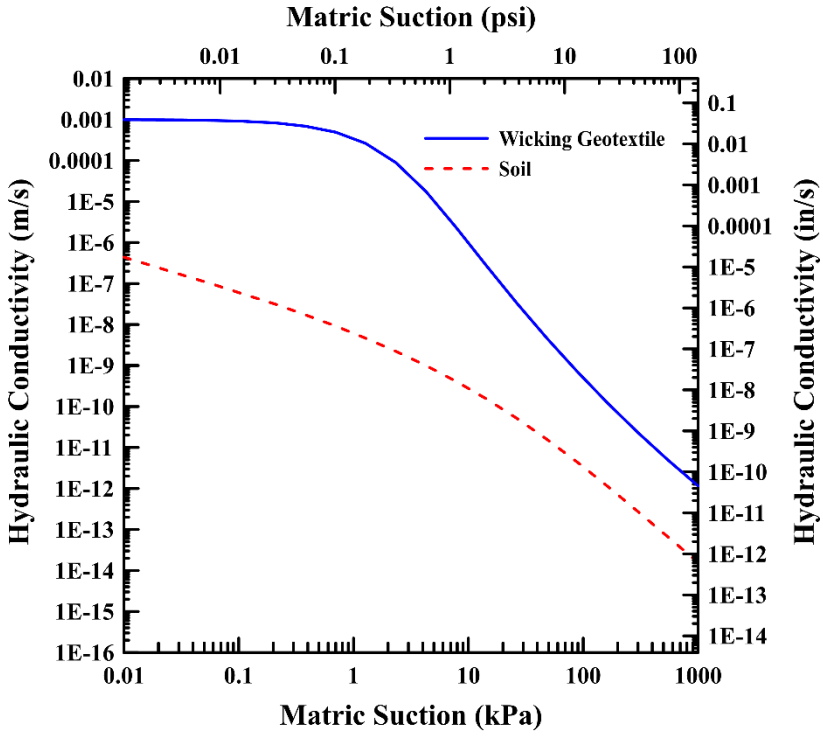

Figure 19. Permeability curves for soil and wicking geotextile

Model Scenarios

Three scenarios were considered in numerical modeling to evaluate the effectiveness of wicking geotextile in slopes:

- No flooding: In this case, the water table was at initial height and steady-state seepage analysis was performed.
- During flooding: In this scenario, the water level was raised to crest height and steady state seepage was performed.
- After flooding: In this case, transient seepage was conducted due to drawdown of water level after flooding.

The variation of the water level was based on flooding data from Hurricane Beryl, obtained from the National Water Information System operated by the United States Geological Survey (USGS), which can be seen in Figure 20. As the maximum increase of water level during the hurricane was 4 meters, the water table for the flooding condition was kept 4 m above the original water level. After completing the transient seepage analysis, the resulting pore water pressure distributions were utilized for slope stability analysis using the limit equilibrium method. Stability analyses were conducted under three distinct conditions: pre-flooding, during flooding, and post-flooding. The primary variations among these scenarios were the hydraulic boundary conditions and the interface strength properties, which were determined based on experimental test results specific to each case. For each scenario, the factor of safety (FOS) of the slope, both with and without wicking geotextile, was calculated and compared.

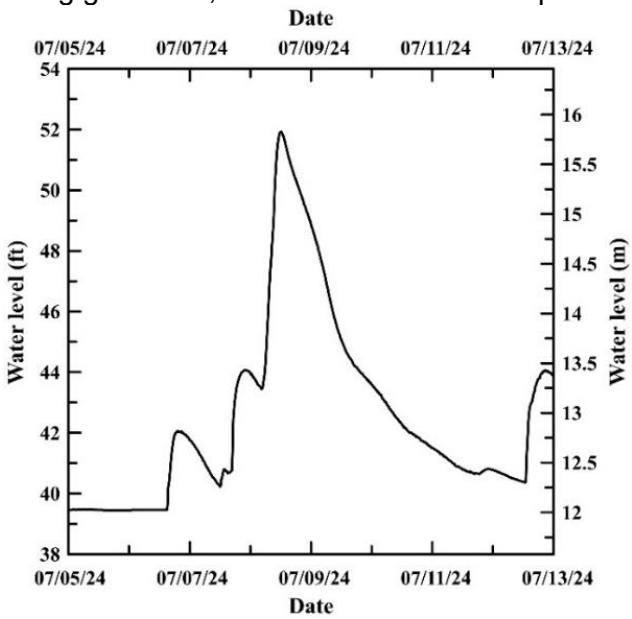

Figure 20. Hurricane Beryl storm surge data

Chapter 4. Results and Discussions

General

This chapter of the report presents and discusses the results of both experimental and numerical studies conducted in this study. Laboratory interface tests were performed under three different hydraulic conditions and results are presented for each condition in the form of stress-displacement plots and shear stress-normal stress plots. The interface properties of wicking geotextile have been presented and the effect of drainage on properties is also discussed. Additionally, the results from drainage tests with and without wicking geotextile are also discussed in this chapter. The specimens for all interface and soil tests were prepared at the target moisture content and dry density, as discussed in the last chapter. The results tabulated in Table 5 show that the measured values were within ±0.6% of the target moisture content, indicating that sample preparation achieved good consistency across tests. In the numerical studies section of this section, both pore water pressure and factor of safety are presented for before, during and after flooding scenarios.

Table 5. Measured initial moisture content of test specimens

	With Geotextile			Without Geotextile		
Stress (kPa)	50	100	200	50	100	200
No Flooding	15.2%	15.0%	15.1%	15.4%	15.3%	15.8%
During Flooding	15.0%	15.8%	15.6%	16.1%	15.1%	14.9%
After Flooding	15.4%	15.0%	15.2%	15.5%	15.1%	16.3%

Interface Tests – At OMC Conditions

Under no flooding condition, three tests were conducted on soil specimens without geotextile at followed by three tests on soil specimens with wicking geotextile at the similar normal stress levels. The experimental results for soil with and without wicking geotextile are presented and compared in Figures 21 and 22. The shear strength-displacement curves did not show a clear peak in shear strength but instead indicated a sharp initial increase in shear strength, followed by a slower rise at larger strains for both the cases. When comparing the two groups of results, at 50 kPa, the soil specimen without geotextile exhibited higher shear stress resistance than the specimen with geotextile. At 100 kPa, the final shear stress values were similar for both tests, while at 200 kPa, the soil with geotextile demonstrated higher shear strength compared to the unreinforced soil. This trend is evident in the normal stress vs shear stress plots, which determines interface strength parameters of soil and wicking geotextile.

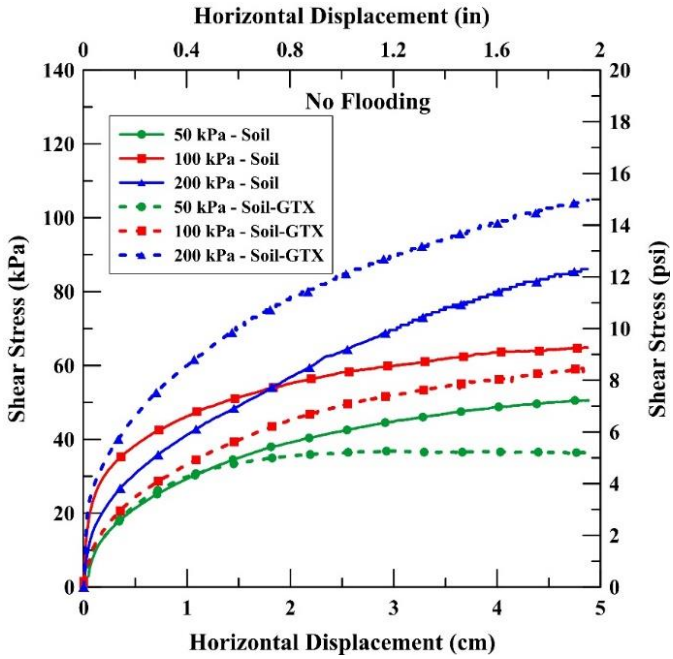

Figure 21. Strength-displacement curves before flooding

The cohesion intercept of soil without geotextile was found to be 40 kPa, higher than the geotextile interface adhesion value of 13 kPa. However, the friction angle at the soil-geotextile interface was greater than the friction angle of the control soil. This indicates that the strength of the soil with geotextile is lower than that of the soil without it when normal stress is below 120 kPa, but higher when normal stress exceeds 120 kPa. The higher friction angle of the soil reinforced with wicking geotextile as compared to the control soil was likely because of interlocking of the wicking fibers and the soil, which took place during the shearing stage. Indentation of geotextile on the soil were visible after the test was completed (Figure 23).

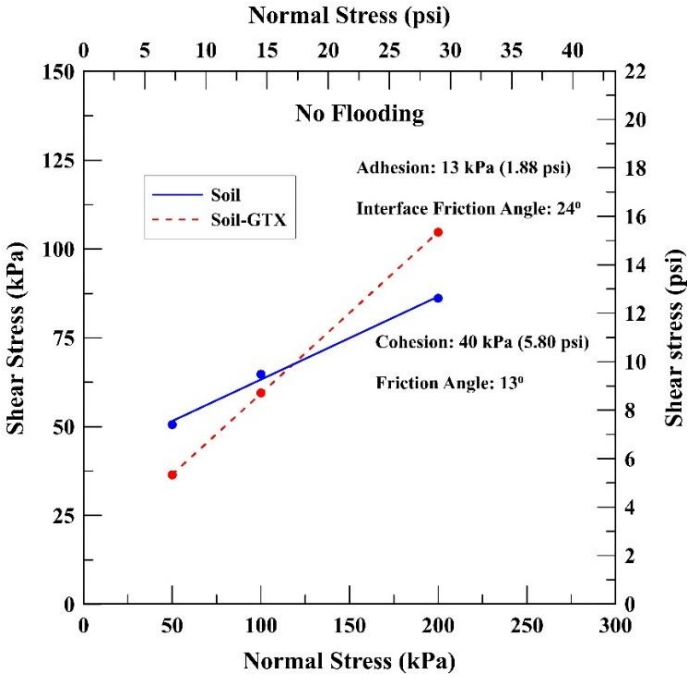

Figure 22. Interface shear parameters before flooding

Figure 23. Grooves from geotextile in soil after test

Interface Tests – During Flooding

In this scenario, interface tests were conducted with lower shear box filled with water simulating flooding condition. The experimental results obtained for soil with and without wicking geotextile are presented and compared in Figures 24 and 25. In both cases, there was a significant loss of strength compared to the tests conducted without flooding. The most notable reduction was observed in the soil cohesion and interface adhesion values. Specifically, soil cohesion decreased from 40 kPa to 14 kPa, while the geotextile interface adhesion value dropped from 13 kPa to 2 kPa. This decline was attributed to a decrease in matric suction caused by flooding and soil saturation, which in turn lowered the shear strength of the soil. However, the friction angle remained largely unchanged in both cases, indicating that the flooding event did not affect either the soil's friction angle or the soil-geotextile interface friction angle.

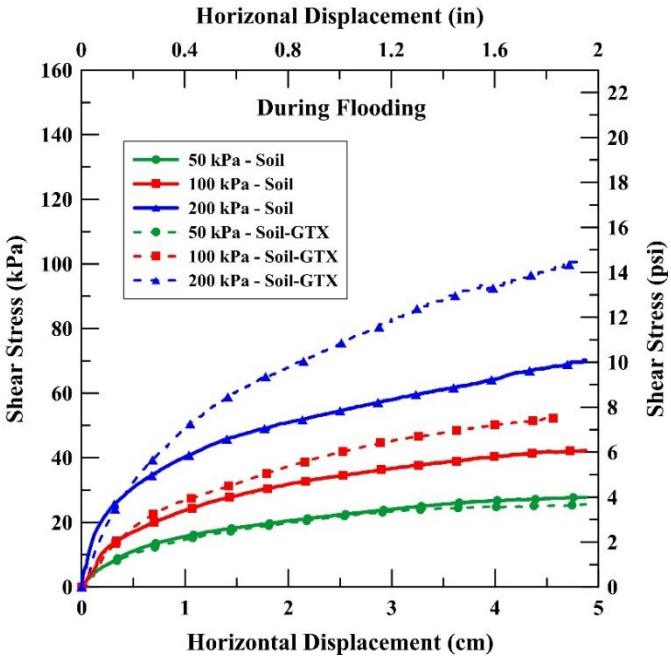

Figure 24. Stress-displacement curves during flooding

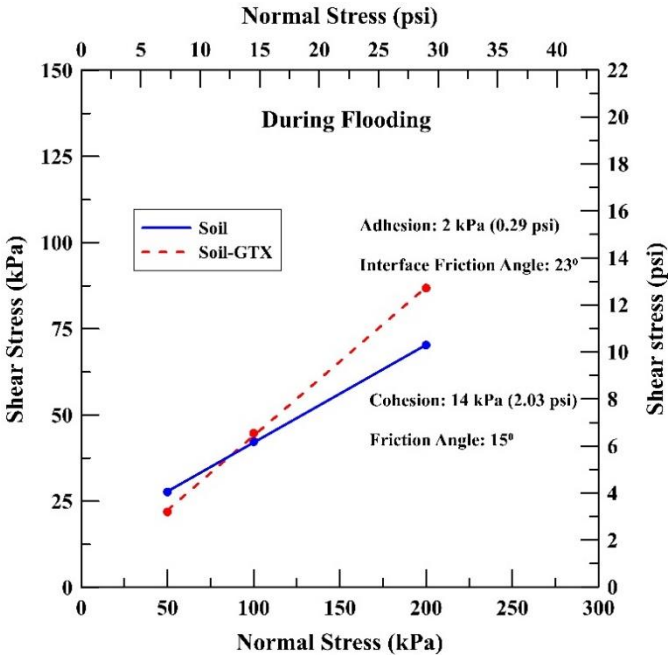

Figure 25. Interface shear parameters during flooding

Interface Tests – 7 Days After Flooding

After 7 days of drainage, the specimens were subjected to shearing, and the resulting stress-displacement curves are presented in Figure 26. The results of tests conducted under flooding condition were also plotted in the same graph to understand the effect of wicking induced drainage on stress-strain curves. Results clearly highlight an increase in shear strength of soil-geotextile interface due to 7 days of drainage. The effect was pronounced in the case test performed at 50 kPa normal stress. This is because the strength increase in this case is

attributed to the rise in adhesion rather than to the strength resulting from the interface friction angle, which is dependent on normal stress. The results plotted in Figure 27 suggest that there was no change in interface friction angle due to drainage. Based on the results, adhesion increased from 2 kPa to 16 kPa after 7 days of drainage. As the soil desaturates, the air-water interface within the soil pores changes, resulting in higher matric suction. The increased matric suction enhances the bonding between soil particles, leading to greater adhesion at the soil-geotextile interface. While wicking-induced drainage may not significantly change the interface friction angle, its impact on adhesion through increased matric suction is notable.

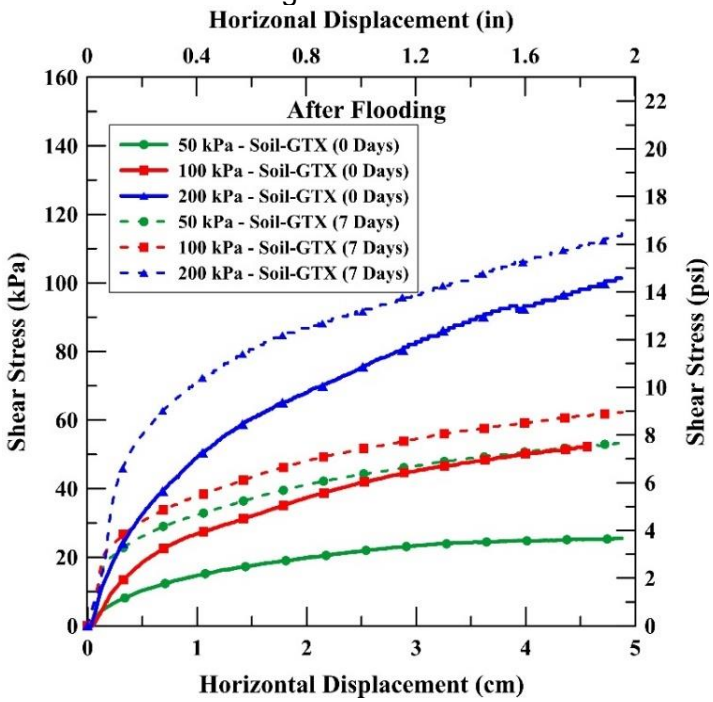

Figure 26. Stress-displacement curves for wicking geotextile during and after flooding

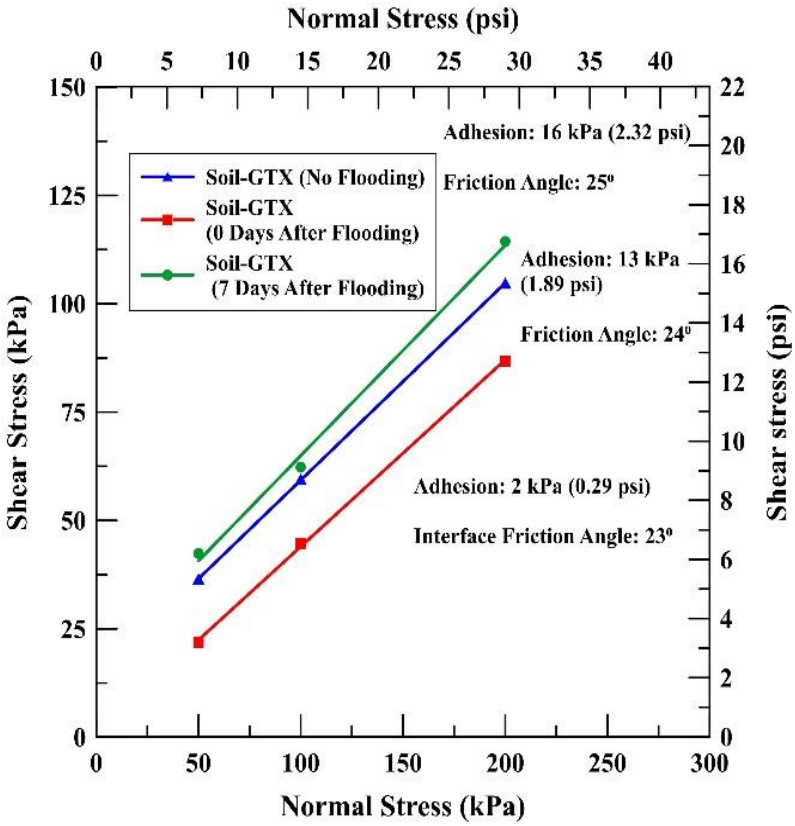

Figure 27. Interface shear properties for wicking geotextile

Summary of Interface Strength Properties

The soil and geotextile interface properties from the direct shear tests under different flooding conditions are summarized in Table 6.

Table 6. Summary of strength properties

	With GTX	With GTX	Without GTX	Without GTX
Parameter	Cohesion (kPa)	Friction Angle (º)	Adhesion (kPa)	Interface Friction Angle (º)
No Flooding	13	24	40	13
During Flooding	2	23	14	15
7 Days After Flooding	16	25	5	25

Moisture Content Variation

The results from 7 days of moisture content data collection are presented in Figure 28. The data reveals that for all three tests without geotextiles, the moisture content remained virtually unchanged throughout the testing period. In contrast, soil specimens with wicking geotextile showed a significant reduction in moisture content across all three tests. The moisture content decrease was most pronounced in the initial days of the tests when the soil was wetter. However, it is important to note that drainage continued even as the soil became desaturated, with the rate of drainage slowing over time. The moisture content reduction observed in the sensors aligns with the direct shear data, which showed improved soil-geotextile interface

parameters, likely due to the desaturation of the soil caused by the wicking action of the geotextile.

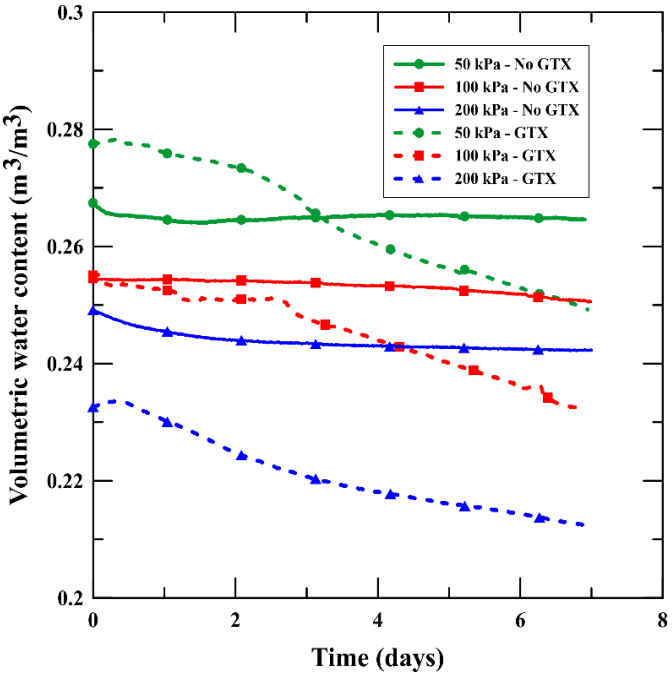

Figure 28. Volumetric water content results from moisture sensors

The tests also indicated that higher normal stress correlated with lower initial moisture content. This is because increased pressure displaces water molecules towards areas of the soil more exposed to the atmosphere, facilitating easier drainage. However, this relationship may also be influenced by other factors, as slight variations in initial water content can result from differences in the soil preparation process or any drainage that occurs between soil preparation and the start of the test. Additionally, based on the total moisture content variations shown in Figure 29, the average gravimetric water content reduction over 7 days was approximately 1.5% for the soil with geotextile, compared to 0.25% for the soil without geotextile.

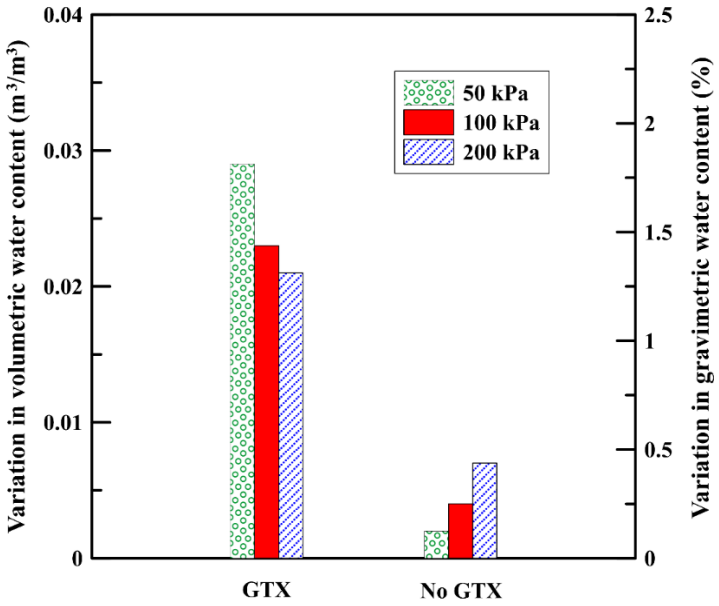

Figure 29. Change in moisture content of soil with and without wicking geotextile

Numerical Study – Before Flooding

Figure 30 represents the pore water pressure contours for Slope 1 with four reinforcement layers. As this is the initial case, only steady state seepage analysis was carried out and as expected, pore water pressure contours were the same for all slopes and reinforcement configurations.

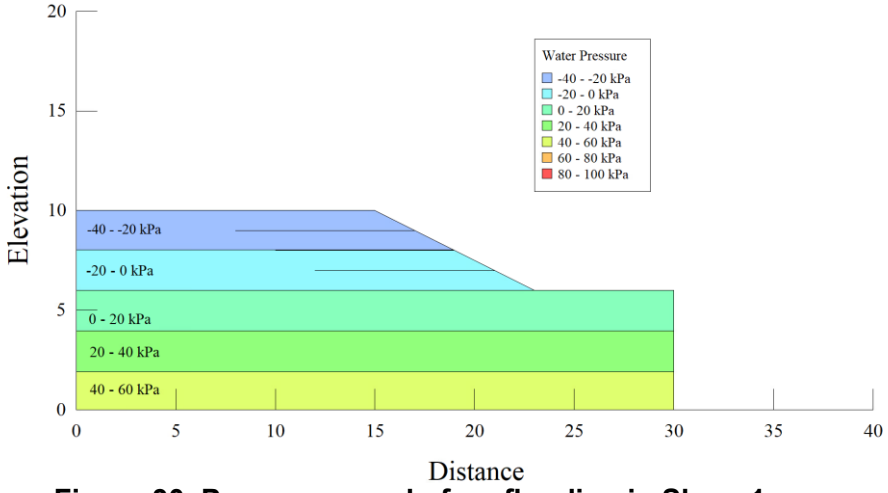

Figure 30. Pore pressure before flooding in Slope 1

The results presented in Figures 31 and 32 show an increase in the Factor of Safety (FOS) for Slope 1, from 2.58 to 2.68. This improvement in FOS is attributed to the pullout resistance and tensile strength properties of the geotextile. It is important to note that the failure surface is deep in both scenarios, which may reduce the effectiveness of the geotextile. However, the failure surface was deeper with the geotextile compared to the unreinforced slope, indicating that the addition of the geotextile shifted the optimal failure surface behind the geotextile layers. Since the failure surface without the geotextile was very deep, not all layers of the geotextile were able to mobilize pullout shear resistance to fully stabilize the slope.

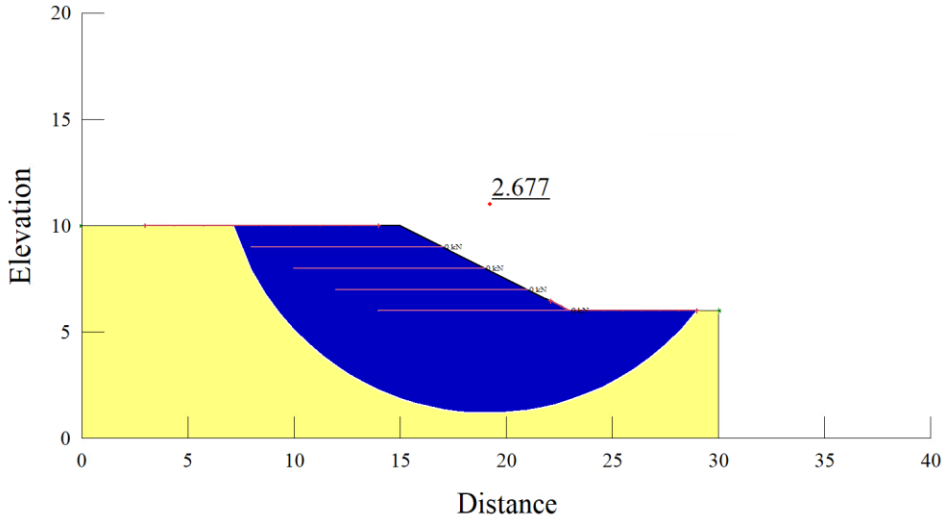

Figure 31. Slope stability for reinforced Slope 1 before flooding

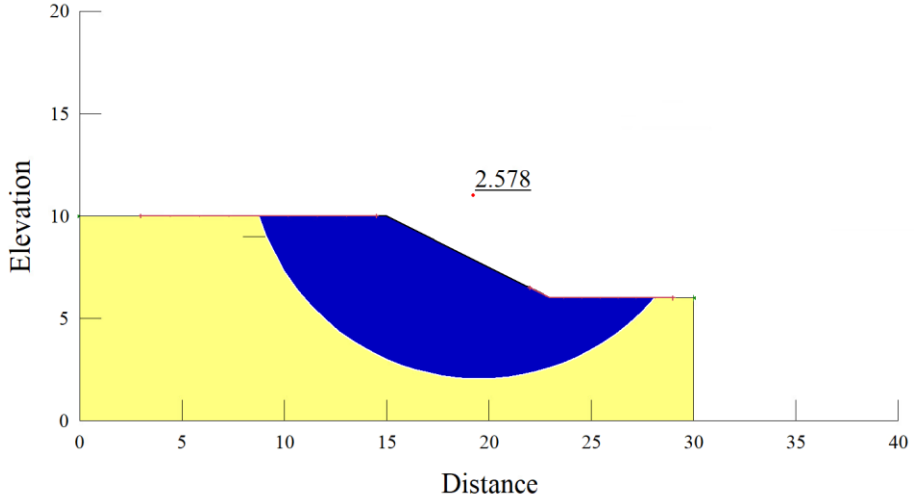

Figure 32. Slope stability for unreinforced Slope 1 before flooding

Numerical Study – During Flooding

To simulate flooding, water level was raised to crest level of the slope. The pore water pressure contour after the steady state seepage with water level at crest is shown in Figure 33. During flooding, since the exposed ends of all layers of geotextile were submerged in water, wicking action of geotextile was not possible. However, there were minor changes in the seepage analysis results caused by the wicking geotextile which did not affect the slope stability. The water content contours in Figure 34 show moisture tends to concentrate around the geotextiles, due to the hydraulic properties of the material.

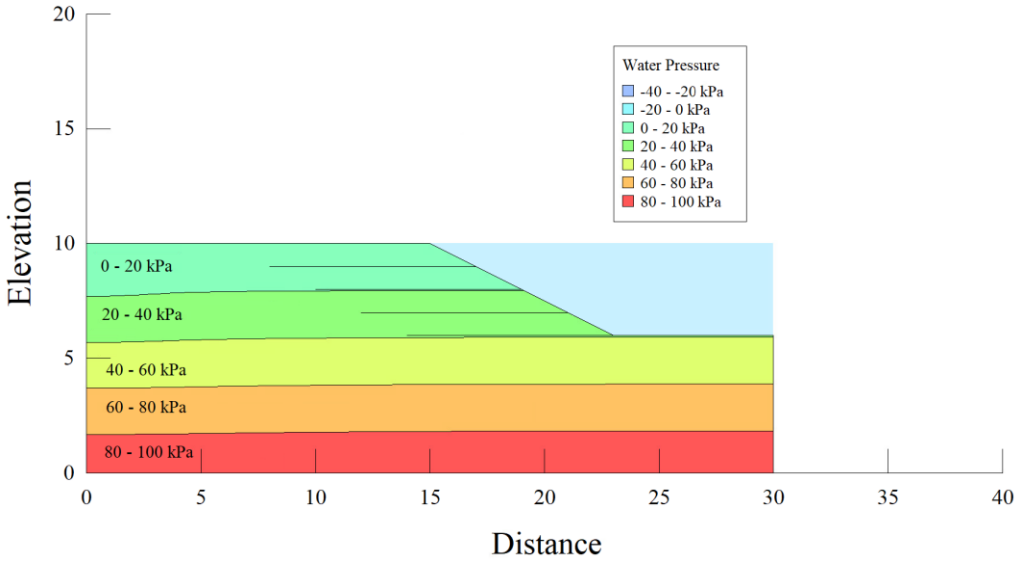

Figure 33. Pore pressure for reinforced Slope 1 before flooding

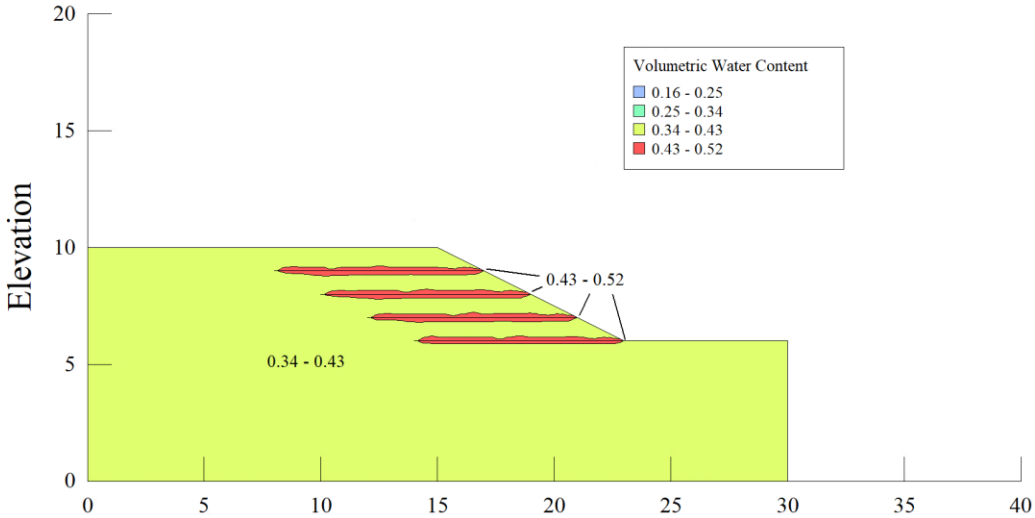

Figure 34. Volumetric water content for reinforced Slope 1 during flooding

During flooding, the presence of water acted as a counterweight, preventing slope collapse, even though the soil was significantly weaker. This resulted in a higher FOS in both cases compared to the no-flooding scenario. As previously noted, wicking action was absent under these conditions, and the improvement in FOS from 3.51 to 3.79 was primarily due to the reinforcement provided by the wicking geotextile. The slope stability results for both the reinforced and unreinforced cases, including the slip surfaces, are shown in Figures 35 and 36.

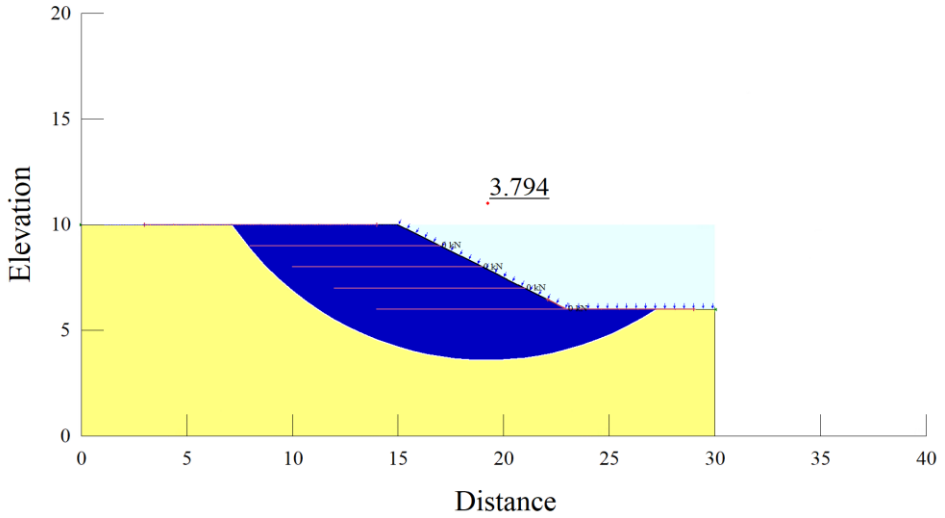

Figure 35. Slope Stability for reinforced Slope 1 during flooding

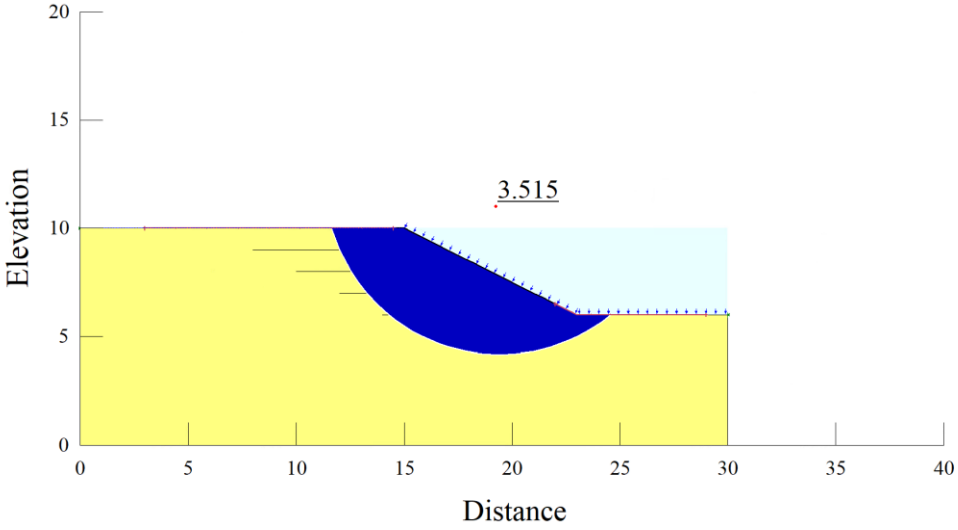

Figure 36. Slope stability for unreinforced Slope 1 during flooding

Numerical Study – After Flooding

After the flooding, the water level returned to its original level within 4 days. During and after the drawdown, water began to seep out from the slope, leading to the desaturation of the soil. In the reinforced slope, water drained horizontally along the wicking geotextile layers, as indicated by the water flux vectors in Figure 37. Most of the drainage occurred around the saturated soil, though some also took place in the upper part of the slope where the soil was unsaturated. In contrast, in the unreinforced case, water did not drain laterally. The drainage in the unreinforced slope was slower, resulting in higher pore pressure values. Furthermore, the water content contours show that in the reinforced slope, moisture tends to accumulate around the geotextile layers before being transported horizontally along them. This observation aligns with the findings from the large-scale direct shear tests, where the soil around the wicking geotextile was observed to be wetter as compared to the soil located above and below the wicking geotextile.

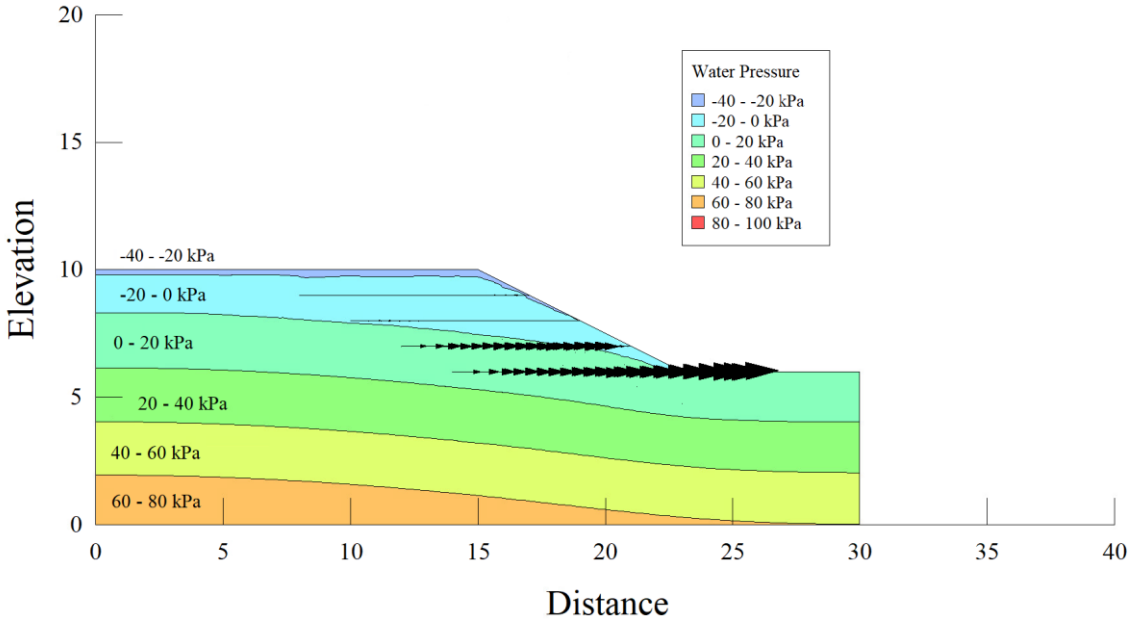

Figure 37. Pore pressure and flow vectors for reinforced Slope 1 after flooding

To further compare the pore water pressure for the reinforced and unreinforced slopes, pore pressure data from the seepage simulation corresponding to Slope 1 with four reinforcement layers was extracted for the second layer of geotextile (Figure 38), and for a point between the second and third layer. From the data, it is possible to make pore pressure vs distance plots for the line and pore pressure vs time plots for the point.

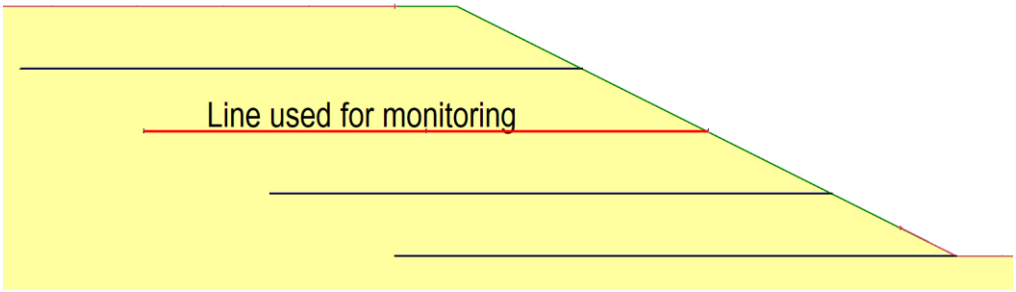

Figure 38. Chosen line for pore pressure monitoring

The pore pressure data shown in Figure 39 establishes that geotextile reinforcement leads to lower water pore pressure within the slope. This difference is more significant between 4 and 9 meters from the slope surface. The exposed end of the geotextile, between 0 and 0.5 meters from the surface, also features a significant change in pore pressure. Furthermore, this pore pressure difference grows as time progresses due to the accumulating effects of wicking action.

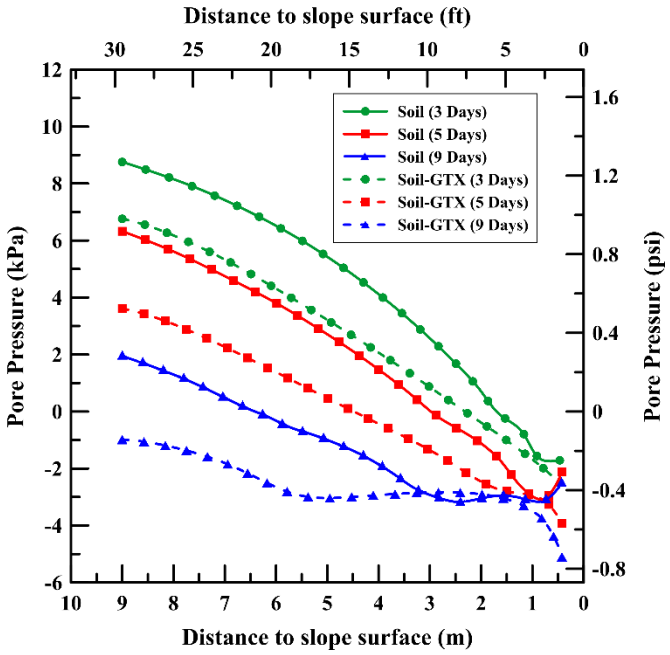

Figure 39. Pore pressure variation over length in Slope 1 with time

As shown in Figure 40, there is an increase in difference between pore pressure in soil in unreinforced and reinforced slopes at the given point due to the drainage facilitated by wicking geotextile. The comparison clearly shows that the wicking geotextile accelerates the reduction in pore water pressure, leading to lower pressure values over time. This suggests more efficient drainage and possibly better stabilization of the slope when geotextile is used.

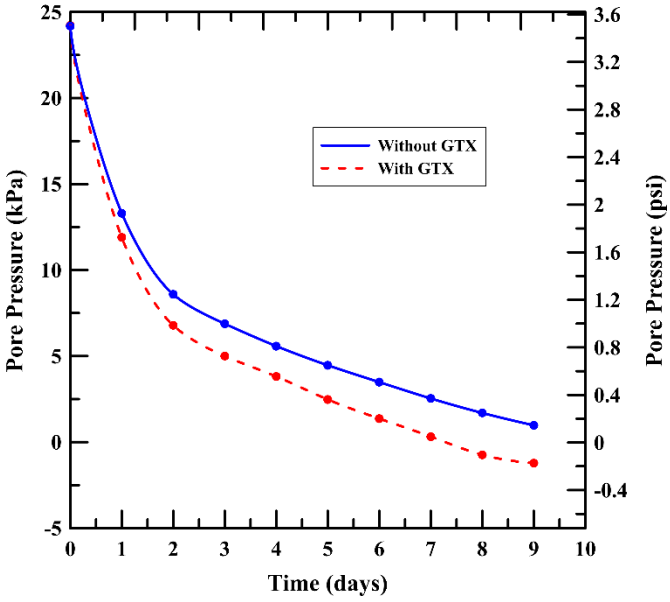

Figure 40. Pore pressure variation over time for chosen point

The drawdown phase following a flooding event is the most critical condition for an embankment slope. After conducting transient seepage analysis during the water level reduction, the Factor of Safety (FOS) for the slope was computed over the next nine days. Immediately after the flooding, the FOS for the reinforced case (Figure 41) was similar to that of the unreinforced case (Figure 42). However, over time, the FOS values began to diverge, highlighting the drainage capability of

the wicking geotextile. This divergence increased, with the difference between the two FOS values becoming greater than before the flooding. The drainage ability of the geotextile enhances the FOS by removing water from the slope and lowering the water table. Unsaturated soil has stronger and more stable strength parameters than saturated soil, which contributes to the increased stability of the slope.

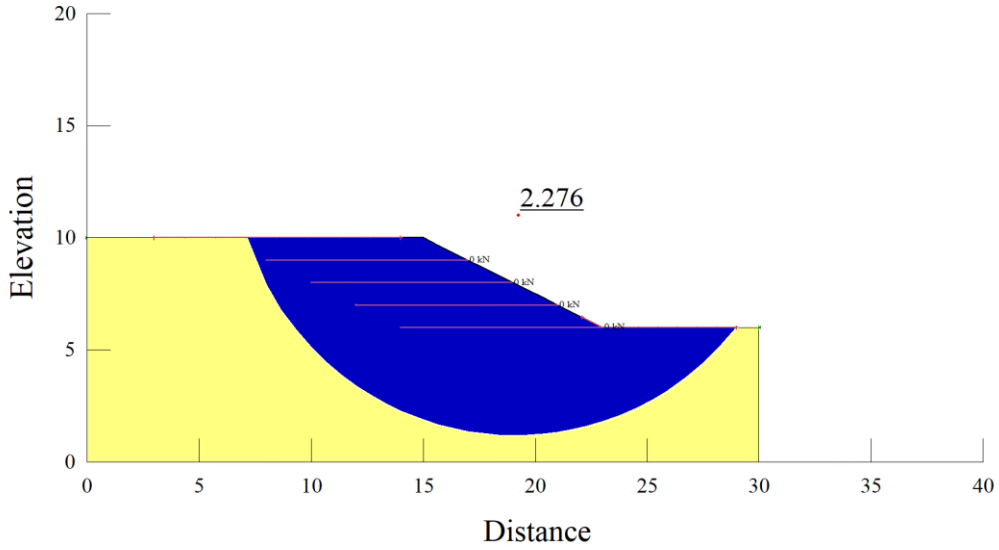

Figure 41. Slope Stability for reinforced Slope 1 after flooding

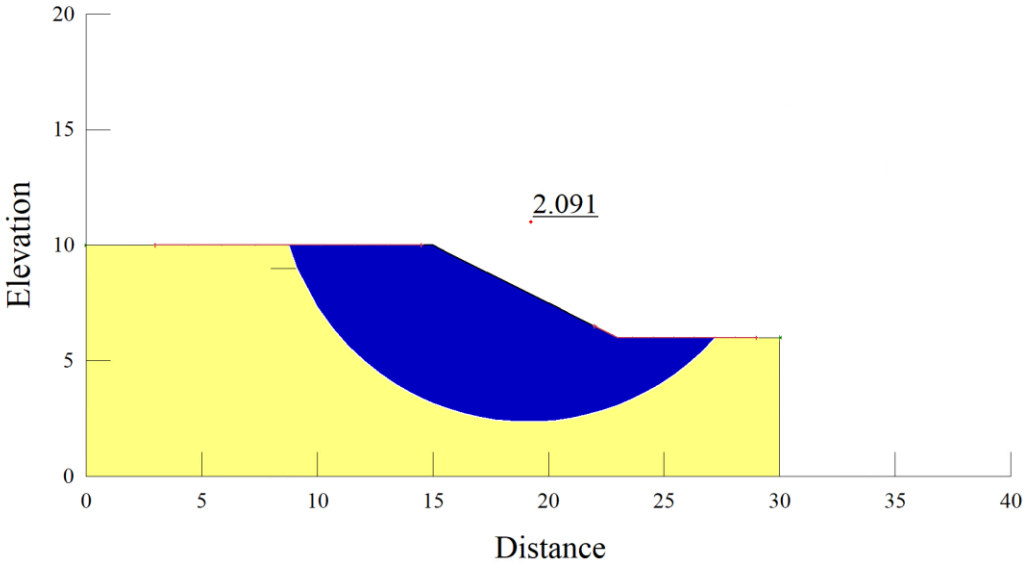

Figure 42. Slope Stability for unreinforced Slope 1 after flooding

For Slope 1, Figure 43 illustrates the variation in the FOS from the flooding condition to 9 days after the water level begins to recede. The lowest FOS occurs 2 days after flooding, when the water table returns to its original level. At this point, the FOS values for both cases are nearly identical, indicating that the moisture levels in the slopes are similar. The slightly higher FOS in the reinforced slope is primarily due to the tensile strength of the geotextile. However, the wicking effect of the geotextile becomes apparent the following day, as evidenced by the growing gap between the two FOS values. This gap demonstrates that most of the wicking action by the geotextile occurs immediately after the water recedes, aligning with the results

from moisture sensors in the laboratory tests, which showed significant reductions in moisture content during the first few days.

From this point, the FOS improves at a similar rate for both the reinforced and unreinforced cases. If the simulation were to continue indefinitely, it is expected that the gap between the two FOS values would eventually narrow to pre-flooding levels, as the slope would continue to drain naturally over time, even without the wicking geotextile. When comparing different reinforcement configurations, the FOS data reveals that two geotextile layers with 2-meter spacing are not very effective at draining the slope, resulting in lower FOS values during the first four days after the drawdown. However, adding more geotextile layers significantly improves the slope's stability. Notably, the FOS results with 8 geotextile layers show only marginal improvement over the 4-layer configuration. This is because the failure surface avoids the geotextile layers in both cases, and four layers are sufficient to effectively drain the slope. A summary of the FOS values before, during, and after flooding is provided in Table 6.

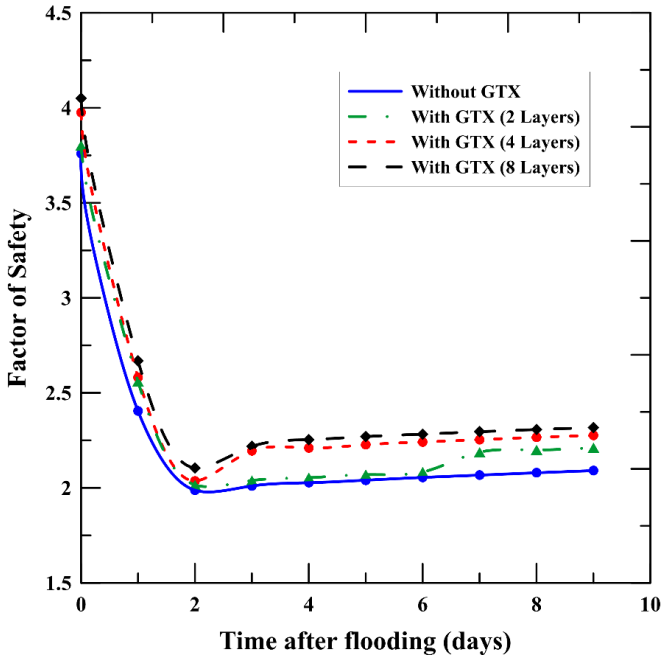

Figure 43. Variation of FOS over time for Slope 1

Table 7. Summary of FOS from Slope 1 stability calculations

	With GTX (Spacing 0.5 m)	With GTX (Spacing 1 m)	With GTX (Spacing 2 m)	Without GTX
Before flooding	2.67	2.68	2.61	2.58
During flooding	3.90	3.79	3.77	3.52
After flooding	2.32	2.28	2.21	2.09

In the case of Slope 2, there were slight reductions in FOS for all reinforcement configurations due to the steeper slope angle, as shown in Figure 44. However, slopes with geotextile reinforcement experienced a smaller reduction in FOS compared to the unreinforced slope, especially immediately after the drawdown. This indicates that the reinforced slopes were more stable during the critical period following the flooding event. As with Slope 1, the influence of additional reinforcement layers diminished over time, as drainage from the slope was completed in all reinforced configurations. The FOS values for all flooding scenarios and reinforcement configurations in this slope are summarized in Table 7.

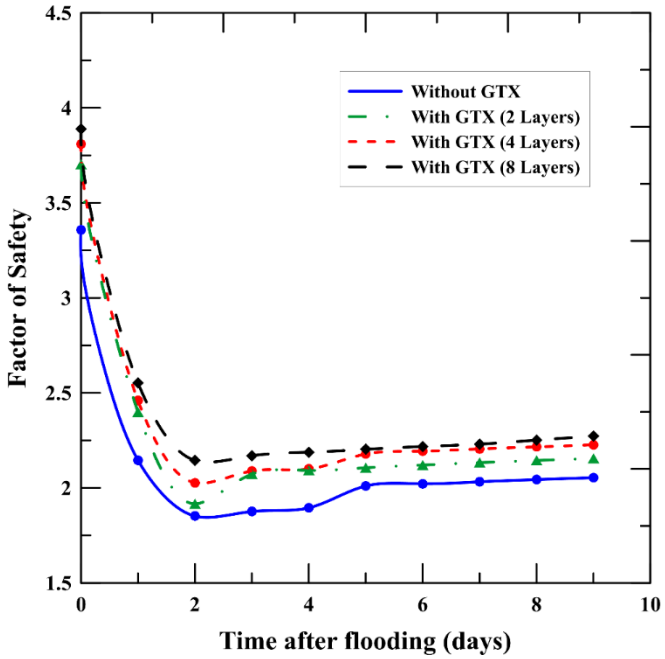

Figure 44. Variation of FOS over time for Slope 2

Table 8. Summary of FOS from Slope 2 stability calculations

	With GTX (Spacing 0.5 m)	With GTX (Spacing 1 m)	With GTX (Spacing 2 m)	Without GTX
Before flooding	2.63	2.61	2.55	2.53
During flooding	3.71	3.71	3.66	3.23
After flooding	2.25	2.23	2.16	2.05

The analysis results for Slope 3, summarized in Figure 45, reveal that the FOS values for reinforced slopes are largely unaffected by the increase in slope angle, in contrast to Slope 1 and Slope 2. However, a significant decrease in FOS is observed for the unreinforced slope. Despite the lowest FOS remaining above 1.5, indicating that the slope is unlikely to fail, it clearly demonstrates vulnerability to flooding events. In contrast, the drainage function of the wicking geotextile maintains the stability of the reinforced slopes. All FOS values for this slope are presented in Table 8.

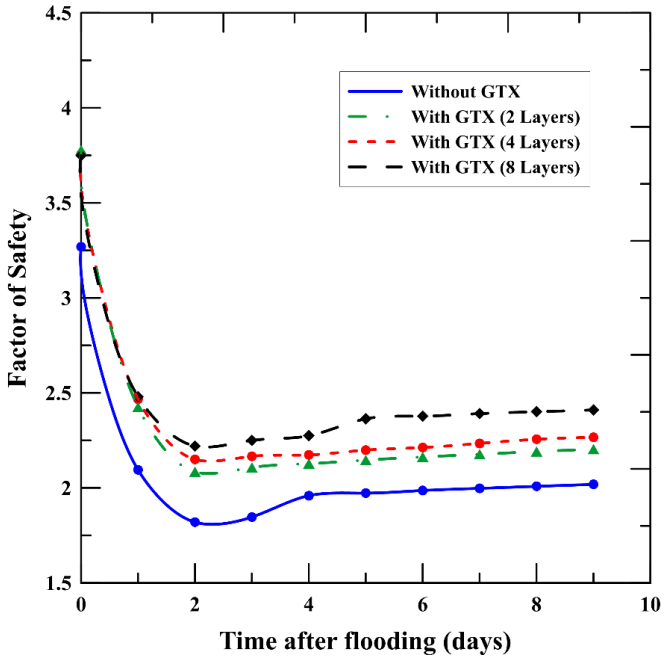

Figure 45. Variation of FOS over time for Slope 3

Table 9. Summary of FOS from Slope 3 stability calculations

	With GTX (Spacing 0.5 m)	With GTX (Spacing 1 m)	With GTX (Spacing 2 m)	Without GTX
Before flooding	2.51	2.51	2.51	2.45
During flooding	3.72	3.63	3.64	2.87
After flooding	2.21	2.2	2.15	2.02

The variation in FOS caused by the change in slope angle for the unreinforced slope and reinforced slope with four geotextile layers, as shown in Figure 46, shows slopes with a steeper angle have lower FOS, which is to be expected. However, the reductions vary significantly between the reinforced and unreinforced slopes. Before flooding, as shown in Figure 49, there is very little decrease in FOS resulting from slope angle for both reinforcement configurations, and the increase brought about by the reinforcement on overall FOS in marginal.

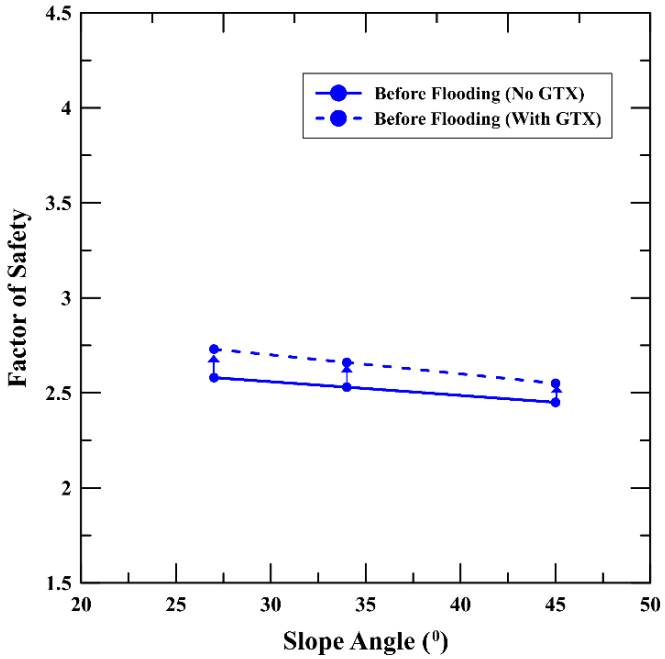

Figure 46. Variation in FOS with slope angle before flooding

Figure 47 shows an increase in FOS occurs during flooding conditions, but the resulting FOS greatly decreases with an increase in slope angle in unreinforced slopes, as opposed to reinforced slopes, which do not experience a significant reduction in FOS.

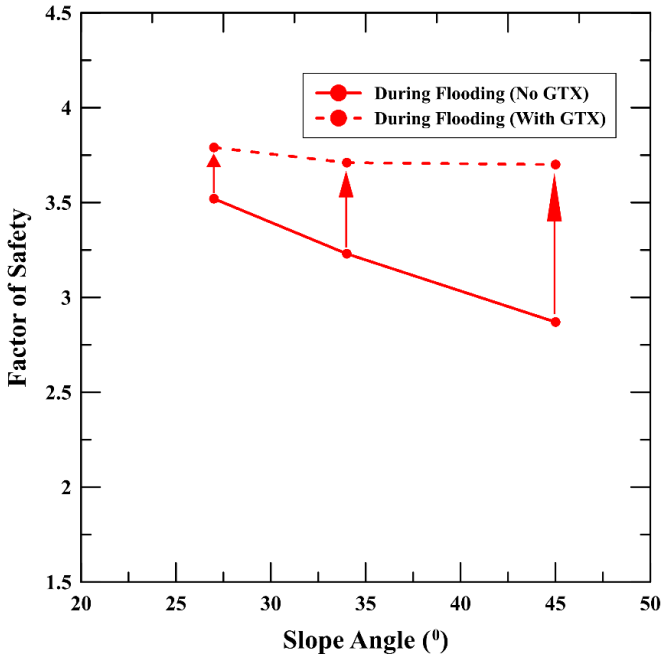

Figure 47. Variation in FOS with slope angle during flooding

Figure 48 shows the FOS values 9 days after flooding. The results indicate that increase in slope angle has little influence on the FOS values of the slope. However, the inclusion of wicking geotextile has increased the FOS values by a margin of approximately 0.5, which

indicates that slope performance during flooding can be enhanced with the inclusion of wicking geotextile.

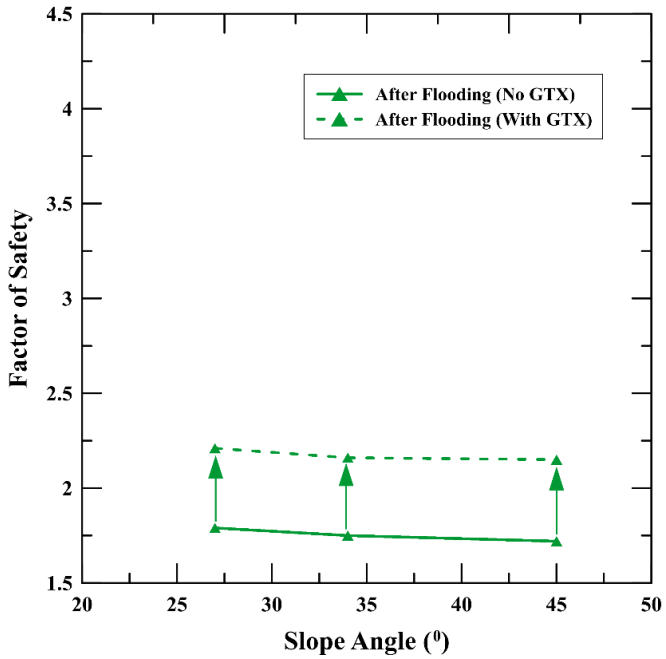

Figure 48. Variation in FOS with slope angle after flooding

Summary of Numerical Studies

Numerical seepage and slope stability analyses were conducted to evaluate the performance of wicking geotextile in embankment slopes with different slope angles and reinforced layers. The simulation results before flooding indicate a minor improvement in the factor of safety due to the strength properties of wicking geotextile because of its higher interface friction angle. In the case of flooding, the failure surface is shallower and there is a considerable improvement in factor of safety due to reinforcement provided by wicking geotextile. Results from the simulation for post flooding event show a gradual improvement in the factor of safety over time for the reinforced slopes compared to the control slopes due to the drainage facilitated by wicking geotextile, which is made evident by the lateral migration of moisture along the geotextile plane and lower pore pressure values in the slope. The simulation results also show an increase in slope angles, causing a slight decrease in factor of safety in most cases and an ample reduction in FOS for unreinforced slopes during flooding. Additional numerical analyses indicated that about 75% of the improvement in slope stability resulted from the reinforcement effect of the wicking geotextile, while approximately 25% was due to its drainage function. The modest overall increase in the factor of safety reflects the relatively gentle slope geometry used in this study. Nevertheless, the results suggest that the benefits of wicking geotextiles become more significant in steeper slopes or drainage-sensitive conditions, where rapid pore-pressure dissipation is essential for maintaining stability. This finding shows the potential of wicking geotextiles as an effective solution for flood-prone or low-permeability embankments.

Chapter 5. Conclusions and Recommendations

The effectiveness of wicking geotextile in moisture drainage from both saturated and unsaturated road bases is well known from previous research studies. With full knowledge of this capacity in pavements, a methodology was developed to evaluate the performance of wicking geotextile as a reinforcement and drainage element in coastal highway embankments. For a thorough assessment of its performance, both experimental and numerical studies were conducted. A large-scale direct shear apparatus was used to conduct interface tests between wicking geotextile and a locally available silty clayey sand. Results obtained from these tests were then used to develop a 2-D finite element model for transient seepage and slope stability analysis. The main conclusions of this study are outlined as follows.

- The interface testing conducted as part of this project indicated that wicking geotextile reinforcement greatly increases friction angle, while the adhesion of the geotextile interface was lower than the cohesion of the soil.
- The results from large-scale direct shear tests demonstrated a clear reduction in soil cohesion and interface adhesion by flooding. However, there was no noticeable change in the friction angle of the soil or the soil-geotextile interface friction angle due to flooding.
- Results from moisture sensors showed a significant decrease in volumetric water content in the soil due to wicking geotextile over the span of a week, with most of the reduction taking place in the first three days, indicating moisture drainage due to wicking action. On the contrary, sensors installed in the soil without wicking geotextile showed no significant decrease in volumetric moisture content.
- Numerical modeling of a wicking geotextile reinforcement design of an embankment slope revealed that water flows in the direction of the geotextile plane in the reinforced slope, whereas it flows along the failure surface in the unreinforced slope. The moisture drainage caused by the geotextile is higher than the natural drainage from the unreinforced slope, leading to reduced moisture in the slope and a lower water table.
- Wicking geotextile reinforcement contributed to a less saturated slope, which led to lower pore pressure and an improvement in FOS values over time compared to the unreinforced slope, even though the FOS was still lower than before the flooding event after 7 days. As a result, wicking geotextile can be considered a viable option for the dehydration of coastal highway embankment slopes in coastal areas which are threatened by precipitation and storm surge from tropical storms and other severe weather phenomena.
- The findings prioritize the use of wicking geotextiles with high interface friction angles to ensure enhanced slope stability under saturated and unsaturated conditions.
- The cost of the wicking geotextile used in this study is approximately 5% higher than that of a conventional non-wicking geotextile with similar tensile and interface strength properties. Considering the potential for enhanced drainage, and improved performance during flooding, this marginal increase in material cost can be justified for applications where slope stability is sensitive to drainage conditions.

- It also suggests application of wicking geotextiles as part of an integrated flood management strategy for coastal transportation infrastructure to mitigate the effects of storm surges and heavy precipitation.

Chapter 6. Implementation of Project Outputs

This research study assesses the performance of wicking geotextile, and the findings provide valuable insights into the potential applications of wicking geotextiles in coastal transportation infrastructure, particularly for mitigating flood-related impacts. This study provided valuable data on the performance of wicking geotextiles as a drainage and reinforcement element. The experimental and numerical results from this study can be used for integration of wicking geotextiles into the design and maintenance of embankment slopes. The results of this study can inform the development of design guidelines for the use of wicking geotextiles in embankment slopes. Apart from the data collected, the study also documented the methodologies and procedures used for data analysis and establishing correlations between flooding conditions and slope behavior. The numerical modeling conducted in this research study provides a framework for simulating various flooding scenarios and evaluating stability of slope reinforced with wicking geotextile. These models can be employed by engineers to conduct site-specific analyses to evaluate the effectiveness of wicking geotextiles for different soil types and climatic conditions.

Furthermore, the successful completion of this project has paved way for a full-scale field study involving wicking geotextile. The study aims to conduct full-scale field investigations to evaluate the drainage capability of the wicking geotextile in reinforced highway slopes. Test sections will be constructed both with conventional geotextile and wicking geotextile at a selected site in central Texas.

Chapter 7. Technology Transfer and Community Engagement and Participation (CEP) Activities

- Poster Presentation on “Assessment of Wicking Geotextiles for Enhanced Resilience in Coastal Infrastructure Vulnerable to Flooding” was made by Jaime Suarez at Infrastructure Advancement Institute (IAI) Summit, Denton, TX, in August 2024.

- Poster Presentation on “Assessment of Wicking Geotextiles for Enhanced Resilience in Coastal Infrastructure Vulnerable to Flooding” was made by Jaime Suarez at CIR Advisory Panel (CAP) Fall 2024, College Station, TX, in September 2024.

- Podium Presentation titled “Assessment of Wicking Geotextiles for Enhanced Drainage and Reinforcement in Flood-Prone Coastal Highway Slopes” by Jaime Suarez at Transportation Research Board Meeting in Washington D.C. in January 2025.

Chapter 8. Invention Disclosures and Patents, Publications, Presentations, Reports, Project Website, and Social Media Listings

- Journal paper titled “Assessment of Wicking Geotextiles for Enhanced Drainage and Reinforcement in Flood-Prone Coastal Highway Slopes” by Puneet Bhaskar, Jaime Suarez, Darelene Goehl, and A. J. Puppala was submitted and is under review for Transportation Research Record - Journal of Transportation Research Board.

References

Alvarenga, C., Parisa, H. A., & Michael, T. H. (2021). Moisture and soil strength monitoring of a railway embankment remediated with wicking geotextile. In *MATEC Web of Conferences* (Vol. 337, p. 03001). EDP Sciences.

Aude, S. A., Mahmood, N. S., Sulaiman, S. O., Abdullah, H. H., & Al Ansari, N. (2022). Slope Stability and Soil Liquefaction Analysis of Earth Dams with A Proposed Method of Geotextile Reinforcement. *GEOMATE Journal*, 22(94), 102-112.

Azevedo, M., & Zornberg, J. G. (2013, February). Capillary barrier dissipation by new wicking geotextile. In *Panamerican conference on unsaturated soils* (pp. 20-22).

Azevedo, M. M. D. (2012). Anti-capillary barrier performance of wicking geotextiles [Doctoral dissertation, University of Texas at Austin]. UT Campus Repository. https://repositories.lib.utexas.edu/items/41d5d076-18b1-4d42-9bbb-60214c5903fe

Azevedo de Almeida, B., & Mostafavi, A. (2016). Resilience of infrastructure systems to sea-level rise in coastal areas: Impacts, adaptation measures, and implementation challenges. *Sustainability*, *8*(11), 1115.

Bai, M., Liu, Z., Zhang, S., Liu, F., Lu, L., & Zhang, J. (2021). Experimental study on the effect of fabric parameter on drainage performance of wicking geotextile. *Fibers and Polymers*, *22*(7), 2044-2051.

Basudhar, P. K. (2010). Modeling of soil–woven geotextile interface behavior from direct shear test results. *Geotextiles and Geomembranes*, *28*(4), 403-408.

Biswas, N., Puppala, A. J., Khan, M. A., Congress, S. S. C., Banerjee, A., & Chakraborty, S. (2021). Evaluating the performance of wicking geotextile in providing drainage for flexible pavements built over expansive soils. *Transportation Research Record*, *2675*(9), 208-221.

Boluk, B., Puppala, A. J., Chakraborty, S., & Bhaskar, P. (2021). Forensic analyses and rehabilitation of a failed highway embankment slope in Texas. *Transportation Research Record*, *2675*(8), 121-134.

Briggs, K. M., Loveridge, F. A., & Glendinning, S. (2017). Failures in transport infrastructure embankments. *Engineering Geology*, *219*, 107-117.

Galinmoghadam, J., Liu, J., Zhang, X., Lin, C., & Guo, Y. (2022). Mitigating pumping in pavement shoulder using wicking geotextile: an experimental study. *Transportation Research Record*, *2676*(11), 145-159.

Guo, J., Wang, F., Zhang, X., & Han, J. (2017). Quantifying water removal rate of a wicking geotextile under controlled temperature and relative humidity. *Journal of Materials in Civil Engineering*, *29*(1), 04016181.

Holland, G., & Bruyère, C. L. (2014). Recent intense hurricane response to global climate change. *Climate Dynamics*, *42*, 617-627.

Idrus, J., Hamzah, N., Ramli, R., Nujid, M. M., & Sadikon, S. F. (2023). Enhancing Slope Stability with Different Slope Stabilization Measures: A Case Study using SLOPE/W Software. *Jurnal Kejuruteraan*, *35*(6), 1427-1434.

Jiang, Y., Alajlan, Z., Zapata, C., & Yu, X. (2024). A Multiphysics Simulation of the Effects of Wicking Geotextile on Mitigating Frost Heave under Cold Region Pavement. *Geosciences*, *14*(2), 34.

Johnston, I., Murphy, W., & Holden, J. (2021). A review of floodwater impacts on the stability of transportation embankments. *Earth-Science Reviews*, *215*, 103553.

Khoury, C. N., Miller, G. A., & Hatami, K. (2011). Unsaturated soil–geotextile interface behavior. *Geotextiles and Geomembranes*, *29*(1), 17-28.

Kumar, S., & Roy, L. B. (2022). Rainfall induced geotextile reinforced model slope embankment subjected to surcharge loading: a review study. *Archives of Computational Methods in Engineering*, 1-19.

Lee, K. M., & Manjunath, V. R. (2000). Soil-geotextile interface friction by direct shear tests. *Canadian geotechnical journal*, *37*(1), 238-252.

Lin, C., Galinmoghadam, J., Han, J., Liu, J., & Zhang, X. (2021). Quantifying and incorporating the benefits of wicking geotextile into pavement design. *Journal of Transportation Engineering, Part B: Pavements*, *147*(3), 04021044.

Lin, C., Presler, W., Zhang, X., Jones, D., & Odgers, B. (2017). Long-term performance of wicking fabric in Alaskan pavements. *Journal of Performance of Constructed Facilities*, *31*(2), D4016005.

Lin, C., & Zhang, X. (2018). Laboratory drainage performance of a new geotextile with wicking fabric. *Journal of Materials in Civil Engineering*, *30*(11), 04018293.

Lin, C., Zhang, X., & Han, J. (2019). Comprehensive material characterizations of pavement structure installed with wicking fabrics. *Journal of Materials in Civil Engineering*, *31*(2), 04018372.

Lin, C., & Zhang, X. (2015). Review of the characterization of geotextile hydraulic behavior. *Innovative Materials and Design for Sustainable Transportation Infrastructure*, 213-221.

Lopes, M. L., & Silvano, R. (2010). Soil/geotextile interface behaviour in direct shear and pullout movements. *Geotechnical and geological engineering*, 28, 791-804.

Luo, L., Guo, J., Chen, A., & Wen, W. (2024, May). Experimental evaluation of one and two-directional wicking geotextile stabilized permeable base. In *IOP Conference Series: Earth and Environmental Science* (Vol. 1335, No. 1, p. 012014). IOP Publishing.

Morgenstern, N. U., & Price, V. E. (1965). The analysis of the stability of general slip surfaces. *Geotechnique*, *15*(1), 79-93.

Mounes, S. M., Karim, M. R., Mahrez, A., & Khodaii, A. (2011). An overview on the use of geosynthetics in pavement structures. *Scientific Research and Essays*, *6*(11), 2234-2241.

Müller, W. W., & Saathoff, F. (2015). Geosynthetics in geoenvironmental engineering. *Science and technology of advanced materials*, *16*(3), 034605.

Neumann, J. E., Price, J., Chinowsky, P., Wright, L., Ludwig, L., Streeter, R., ... & Martinich, J. (2015). Climate change risks to US infrastructure: impacts on roads, bridges, coastal development, and urban drainage. *Climatic Change*, *131*, 97-109.

Pal, I., Kumar, A., & Mukhopadhyay, A. (2023). Risks to coastal critical infrastructure from climate change. *Annual Review of Environment and Resources*, *48*(1), 681-712.

Poshti, M. R. T. (2020). Geotextiles in Filtration and Drainage Applications in Embankment Dams: Technical Examination and Analysis of Effects. *World Journal of Environmental Biosciences*, *9*(1-2020), 96-105.

Qian, Z., & Rahardjo, H. (2016). Application of fitting parameters in best fit equation.

Salahudeen, A. B., & Yisa, G. L. (2023). Settlement, slope stability and seepage analyses By Numerical Modelling Method and their applications in practice. *Nigerian Journal of Technology*, *42*(3), 306-314.

Sharar-Salgado, D. S., & Brown, E. R. (2023). Resources for Understanding Challenges and Opportunities for Coastal Highway Projects. *Public Roads*, *87*(2).

Tan, Y. L., Cao, J. J., Xiang, W. X., Xu, W. Z., Tian, J. W., & Gou, Y. (2023). Slope stability analysis of saturated–unsaturated based on the GEO-studio: a case study of Xinchang slope in Lanping County, Yunnan Province, China. *Environmental Earth Sciences*, *82*(13), 322.

Tate, C., & Frazier, T. (2013). A GIS methodology to assess exposure of coastal infrastructure to storm surge & sea-level rise: a case study of Sarasota County, Florida. *J Geogr Nat Disasters*, *1*, 2167-0587.

Xie, X., Yang, G., Liu, Z., Tang, Y., Chu, J., Wen, W., ... & Luo, L. (2024). Field experiment on a vegetation-wicking geotextile-reinforced base for a permeable sidewalk. *Frontiers in Built Environment*, *10*, 1333937.

Zaman, M. W., Han, J., Kabir, M. U., & Parsons, R. L. (2024). Laboratory evaluation of wicking geotextile for moisture reduction in silty sands at different fines contents. *Geotextiles and Geomembranes*, *52*(6), 1180-1190.

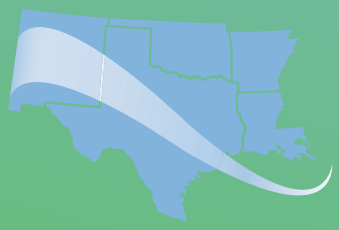

SOUTHERN PLAINS
TRANSPORTATION CENTER

The University of Oklahoma | OU Gallogly College of Engineering
202 W Boyd St, Room 213A, Norman, OK 73019 | (405) 325-4682 | Email: sptc@ou.edu